Quantum kinetics of a two-component 1D Fermi gas using the G1–G2 scheme: Collision properties of a particle beam in a dense plasma

by

Francisco Borges Fajardo

Erster Gutachter: Prof. Dr. Michael Bonitz

Zweiter Gutachter: Priv.-Doz. Dr. Hanno Kählert

Abstract

One of the greatest achievements in computational many-body physics is the possibility to understand and describe correlation effects. Long time it was difficult to calculate correlation because of the high demand in computational power, but with the progress of technology and more modern theoretical methods the calculations are finally possible. These quantum properties on a microscopic level can be investigated and used to understand macroscopic effects. Thus, a large number of interacting particles, such as in solids, liquids and plasmas, can be explained and predicted. Finally, these predictions can be verified in an experiment. In fact, condensed matter physics is one of the most active fields of physics, because of it's industrial applications. In this thesis, the newly developed quantum kinetic equations in the framework of non-equilibrium Green's function (NEGF), the G1–G2 scheme [1][2], will be used, which is based on the Generalized Kadanoff-Baym Ansatz (GKBA).

The G1–G2 scheme achieves linear time scaling, because in contrast to the GKBA, which incorporates the correlation effects through the memory integral, the G1–G2 scheme eliminates the memory effect by introducing the equation of motion (EOM) for the two-particle non-equilibrium Green's function (2pNEGF) that leads to a time local description. In this thesis, the correlation effects will be taken into account with second order approximation (SOA) for the self-energy. Further, the aim of this thesis is to study under which criteria/criterion collisions between particles in an, one-dimensional fermionic quantum plasma for the given approximation emerge. It can be shown for SOA that the velocity difference is the key quantity that needs to be considered, which will be derived in section 4.2. It was found that if the velocity difference between colliding particles goes to zero, then the scattering probability is maximal. Finally, different plasma configurations will be tested and discussed to further verify the criterion that are made.

Zusammenfassung

Eine der größten Errungenschaften der computergestützten Vielteilchenphysik ist die Möglichkeit, Korrelationseffekte zu verstehen und zu beschreiben. Es ist schwer Korrelation zu berechnen, weil es rechentechnisch anspruchsvoll ist. Mit dem Fortschritt der Technologie und neuen modernen theoretischen Methoden sind die Berechnungen möglich. Mit diesen lassen sich Quanteneigenschaften auf mikroskopischer Ebene untersuchen und können benutzt werden, um makroskopische Effekte zu verstehen. Eine große Anzahl an wechselwirkenden Teilchen, wie man sie in Festkörpern, Flüssigkeit und Plasmen auffindet, können erklärt und vorhergesagt werden. Diese Vorhersagen können anschließend experimentell bestätigt werden. Aufgrund des industriellen Nutzens, ist die Physik der kondensierten Materie, eins der größten aktiven physikalischen Bereiche die es gibt. In dieser Arbeit werden die neu entwickelten quantenkinetischen Gleichungen, im Rahmen der Nichtgleichgewichts-Green Funktion (NEGF), das G1–G2 Schema angewendet, welches auf dem generalisierten Kadanoff-Baym Ansatz (GKBA) basiert. Das G1–G2 Schema [1][2] erreicht lineare Zeitskalierung, da im Gegensatz zum GKBA, welches Korrelationseffekte in dem Gedächtnisintegral berücksichtigt, der Gedächtniseffekt beseitigt wird, in dem eine Bewegungsgleichung (EOM) für die zwei-Teilchen Nichtgleichgewichts-Green Funktion (2pNEGF) eingeführt wird. Dies führt zu einer zeitlokalen Beschreibung. Korrelationseffeke werden in dieser Arbeit mit der Selbstenergie in zweiter Bornschen Näherung berücksichtigt. Desweiteren ist das Ziel zu untersuchen unter welcher Bedingung Stöße zwischen Teilchen in einem eindimensionalen fermionischen Quantenplasma in gegebener Näherung entstehen. Es konnte gezeigt werden, dass in zweiter Bornscher Näherung die Geschwindigkeitsdifferenz die wichtigste Größe ist, welche in Sektion 4.2 hergeleitet wird. Es wurde erkannt, dass wenn die Geschwindigkeitsdifferenz zwischen streuenden Teilchen gegen Null geht, die Streuwahrscheinlichkeit maximal ist. Abschließend werden verschiedene Plasmakonfigurationen getestet und diskutiert, um das Stoßkriterium zu verifizieren.

Contents

1 Introduction

A plasma becomes degenerate when the thermal De Broglie wavelength is large compared to the average interparticle distance. In this case, quantum effects become relevant, because their wave functions overlap. These quantum plasmas can be found naturally inside some astronomical objects such as neutron stars and brown dwarfs. Furthermore, a quantum plasma can be produced on Earth in laboratories with laser beams of high intensity, which compress the charged particles. Additionally, these kinds of plasmas can be found in solids, like the electron gas in conductors (like in metals) or electron-hole plasma in semi-conductors. To understand solids it is important to understand plasmas. Therefore, an active research field exists. Furthermore, most gaslike plasmas contain more than one charged particle species, nevertheless in laboratory the multi-component plasma can be motivated for inertial confinement fusion, which could generate new possibilities in green energy. Finally, it is believed that the universe right after the Big Bang was in an exotic state of quantum plasma, containing only elementary particles, like photons, quarks and gluons. These particles are produced for fundamental research in particle accelerator for example at CERN, inside the Large Hadron Collider[3].

To describe non-equilibrium quantum plasmas theoretically several formalisms are available, for example the time-dependent Schrödinger equation (TDSE), the time-dependent density functional theory (TDDFT) or quantum kinetic approaches [4] such as the non-equilibrium Green's function Theory (NEGF). The Schrödinger equation scales exponentially with the number of particles, which only enables solutions for a small number of particles. In comparison, the NEGF also scales exponentially with the particle number when N-body collisions need to be considered. Yet we will use NEGF theory due to the fact that the equation of motion, consisting of a hierarchy of coupled equations, enables the possibility to truncate the hierarchy. Suitable approximations can be generated with many-body perturbation theory, such as the diagrammatic techniques and as a result the computing effort can be reduced. Originally, the investigation of stopping power in an one-dimensional two-component plasma was the objective of this thesis, where different particles collide with the bulk and the energy loss of the projectile is investigated. These processes are relevant for many areas of physics such as condensed matter physics and astrophysics, it allows to analyze electronic

1

properties of matter. Recent progresses concerning the creation of doublons in small hexagonal graphene-type clusters caused by ion impact was made [5][6]. It is a different physical situation with different symmetries in comparison to the system presented in this thesis, but the stopping process stays the same. Though, similar homogeneous setups were also considered, such as for example stopping power of an electron bulk and electron particle beam to investigate the influence of dynamical screening [7] in three dimensions. Non-kinetic approaches to stopping power, with the quantum Monte Carlo method are also investigated extensively [8]. Returning to the setup investigated in this thesis: Unfortunately, the first calculations showed no relaxation towards equilibrium. So instead, the collision properties of an one-dimensional two-component gas will be examined to understand the processes of scattering in momentum space. Thus, eventually the opportunity to generate a stopping curve is possible.

1.1   Outline

- **Chapter 1 – Introduction**

- **Chapter 2 – Many-Body Theory**
  First, the transition from first quantization to second quantization is made, a short derivation of the Keldysh-Kadanoff-Baym equation is shown, to further simplify the computational effort, the Generalized Keldysh-Kadanoff-Baym Ansatz is introduced. Finally, the G1–G2 scheme, that scales linear in time is derived and the transition to momentum representation is made.

- **Chapter 2 – Many-Body Theory**
  First, the transition from first quantization to second quantization is made, a short derivation of the Keldysh-Kadanoff-Baym equation is shown, to further simplify the computational effort, the Generalized Keldysh-Kadanoff-Baym Ansatz is introduced. Then the G1–G2 scheme, that scales linear in time is derived. Finally, an brief introduction to jellium is presented and the transition to momentum representation is made.

- **Chapter 3 – Setup**
  In this section some simulation related aspects will be presented. The interaction potential and initial conditions are shown, further some relevant parameters of the simulation and convergence criteria are discussed.

- **Chapter 4 – Results**
  First, a general collision criterion is derived, then the collision criterion is expanded in a power series for free GKBA, for small transfer momentum. Finally, the condition is verified with numerical results.

- **Chapter 5 – Conclusion & Outlook**

2 Many-Body Theory

In this section, the most important mathematical tools to describe many-body theory in the framework of the G1–G2 scheme will be presented. We begin with the formalism of second quantization, where many-body quantum states in occupation numbers representation are key quantities. Further, the two time one-particle non-equilibrium Green's function (1pNEGF) is defined and the equation of motion is formulated. Additionally, the Generalized Kadanoff-baym Ansatz (GKBA) is introduced, which is easier to handle in computational aspects. Then, the G1–G2 scheme will be derived and an introduction to jellium is presented. Then finally, the generalization to multi-component and the transition of the G1–G2 scheme to momentum representation is performed.

2.1 Second Quantization

The complete dynamical information of N-particles is incorporated in the N-particle quantum state $\mid \Psi_N \rangle$[9][10], as the solution of the time-dependent N-particle Schrödinger equation[9]

$$\hat{H}_N \mid \Psi_N \rangle(t) = i\hbar \frac{d}{dt} \mid \Psi_N \rangle(t). \tag{2.1}$$

these states are elements of the N-particle Hilbert space

$$\mathcal{H}_N = \underbrace{\mathcal{H}_1 \otimes \mathcal{H}_1 \otimes ... \otimes \mathcal{H}_1}_{\text{N-times}}, \tag{2.2}$$

which is the direct product of one-particle Hilbert spaces.

Indistinguishable particles are described by (anti-)symmetric states. These states need to behave (anti-)symmetrically under permutation, thus new physical properties arise. A symmetrized state can be identified with bosons and an anti-symmetrized state with fermions, which implies Pauli blocking. We denote by $\Lambda_N^{\pm}\mathcal{H}$ the Hilbert space of these (anti-)symmetric

4

states. In second quantization we define creation and annihilation operators, which changes the particle numbers. The space that supports this is called the Fock space:

$$\mathcal{F}^\pm = \bigoplus_{N=0}^{\infty} \Lambda_N^\pm \mathcal{H}_1^{\otimes N} = \mathbb{C} \oplus \mathcal{H}_1 \oplus \Lambda_2^\pm(\mathcal{H}_1 \otimes \mathcal{H}_1) \oplus \Lambda_3^\pm(\mathcal{H}_1 \otimes \mathcal{H}_1 \otimes \mathcal{H}_1)... , \qquad (2.3)$$

which is the direct sum over (anti-)symmetrized N-particle Hilbert spaces for all particle numbers. The basis states can be constructed with Slater determinants for fermions or permanents for bosons. The Slater determinant and the permanent take indistinguishability into account automatically and the states are fully characterized by the information of the involved single-particle orbitals. In the next step the occupation number representation is introduced, where we expand the Fock state in terms of occupation numbers using the completeness relation

$$\sum_{\{n\}} |\{n\}\rangle \langle\{n\}| = 1. \qquad (2.4)$$

The Fock state takes the following form

$$|\,\Psi\rangle^\pm = \sum_{\{n\}} c_{\{n\}} |\{n\}\rangle^\pm , \qquad (2.5)$$

which is the superposition of Slater determinants (-) or permanents (+). Where $\{n\} = n_1, n_2, n_3, ...$ represents the total set of occupation numbers of all single-particle states and $c_{\{n\}}$ is the expansion coefficient.

Non-Hermitian operators with the following properties are defined: The annihilation operator $\hat{a}_i$ reduces the total particle number by one, by removing a particle in state i. On a simple product state it acts as

$$\hat{a}_i |n_1, n_2, ..., n_i, ...\rangle = \sqrt{n_i} |n_1, n_2, ..., n_i - 1, ...\rangle \cdot \begin{cases} 1 & \text{for bosons} \\ (-1)^\alpha \delta_{n_i,1} & \text{for fermions} \end{cases}. \qquad (2.6)$$

The creation operator $\hat{a}_i^\dagger$ adds a particle in state i to the total number of particles

$$\hat{a}_i^\dagger |n_1, n_2, ..., n_i, ...\rangle = \sqrt{n_i + 1} |n_1, n_2, ..., n_i + 1, ...\rangle \cdot \begin{cases} 1 & \text{for bosons} \\ (-1)^\alpha \delta_{n_i,0} & \text{for fermions} \end{cases}, \qquad (2.7)$$

with $\alpha = \sum_{l=1}^{i-1} n_l$, that incorporated the properties of (anti-)symmetric states. The Kronecker delta in the fermionic expression leads to occupation numbers of each one-particle

state between 0 and 1.

The properties can be written in a condensed form:

$$[\hat{a}_i, \hat{a}_j]_\mp = [\hat{a}_i^\dagger, \hat{a}_j^\dagger]_\mp = 0, \tag{2.8}$$

where a distinction must be made, between bosonic and fermionic annihilation and creation operators. The upper sign on the commutator represents standard commutation relation for bosonic ladder operators and the lower sign represents the anti-commutator for fermionic operators. The third commutator relation is

$$[\hat{a}_i, \hat{a}_j^\dagger]_\mp = \delta_{i,j}, \tag{2.9}$$

with all these mathematical tools defined one can create any arbitrary product state out of vacuum.

$$|n_1, n_2, ...\rangle = \frac{1}{\sqrt{n_1! n_2! ...}} (\hat{a}_1^\dagger)^{n_1} (\hat{a}_2^\dagger)^{n_2} ... |0\rangle . \tag{2.10}$$

Further, the N-particle operator can be defined in second quantization representation as

$$\hat{O}_N = \frac{1}{N!} \sum_{i_1...i_N j_1...j_N=1}^{\infty} o_{i_1...i_N j_1...j_N} \hat{a}_{i_1}^\dagger ... \hat{a}_{i_N}^\dagger \hat{a}_{j_N} ... \hat{a}_{j_1}, \tag{2.11}$$

with the matrix elements $o_{i_1...i_N j_1...j_N} = \langle i_1...i_N | \hat{O} | j_1...j_N \rangle$. For example, the Hamiltonian in second quantization that accounts for one- and two-body contributions becomes

$$\hat{H}(t) = \sum_{ij} h_{ij}^{(0)}(t) \hat{a}_i^\dagger \hat{a}_j + \frac{1}{2} \sum_{ijkl} w_{ijkl}(t) \hat{a}_i^\dagger \hat{a}_j^\dagger \hat{a}_l \hat{a}_k, \tag{2.12}$$

with $h_{ij}^{(0)}(t) = h_{ij}^{\text{kin}} + u_{ij}(t)$. The first term t_{ij} is the kinetic energy matrix element and the second term u_{ij} is the matrix element that accounts for interaction with external fields. The second term on the right-hand side accounts for interaction between particles. The interaction energy can be time-dependent. for example when one start in an uncorrelated state and use adiabatic switching to raise the interaction with time. It needs to be indicated that the Heisenberg picture will be used in the following until otherwise stated. The equation of motion for operators can be found using the Heisenberg equation.

$$i\hbar \frac{d}{dt} \hat{A} = [\hat{A}, \hat{H}] + i\hbar \frac{\partial}{\partial t} \hat{A}, \tag{2.13}$$

with $\hat{A}$ being an arbitrary operator and the second term on the right-hand side accounts, for explicit time dependence, thus the equation of motion for the annihilation and creation operator can be formulated.

$$i\hbar\frac{d}{dt}\hat{a}_i = [\hat{a}_i, \hat{H}] = \sum_k h_{ik}\hat{a}_k + \sum_{mkl} w_{imkl}\hat{a}_m^\dagger\hat{a}_l\hat{a}_k \tag{2.14}$$

$$i\hbar\frac{d}{dt}\hat{a}_i^\dagger = [\hat{a}_i^\dagger, \hat{H}] = -\sum_k h_{ki}\hat{a}_k^\dagger - \sum_{mkl} w_{klim}\hat{a}_k^\dagger\hat{a}_l^\dagger\hat{a}_m \tag{2.15}$$

It can be seen that $\hat{a}_i$ and $\hat{a}_i^\dagger$ obeys a non-linear Schrödinger type equation.

2.2   Non-equilibrium Green's Functions

In this section a more advanced technique for many-body description will be presented, the non-equilibrium Green's Functions (NEGF) Theory[11][12]. For this, the second quantization formalism will be used. The key quantity of this approach is the two time contour ordered ensemble averaged one-particle Green's function (1pNEGF)

$$G_{ij}(z, z') := -\frac{i}{\hbar}\Big\langle \mathcal{T}_\mathcal{C}\big\{\hat{a}_i(z)\hat{a}_j^\dagger(z')\big\}\Big\rangle = \theta_\mathcal{C}(z - z')G_{ij}^>(z, z') + \theta_\mathcal{C}(z' - z)G_{ij}^<(z, z'). \tag{2.16}$$

The time ordering operator $\mathcal{T}_\mathcal{C}$ ensures the correct time ordering of bosonic and fermionic strings of operators on the complex time contour z, which is defined on the Keldysh contour. Two new quantities arise, the greater component

$$G_{ij}^>(z, z') := -\frac{i}{\hbar}\Big\langle \hat{a}_i(z)\hat{a}_j^\dagger(z')\Big\rangle, \tag{2.17}$$

which first creates a new particle in state j to the time z' and at last annihilates a particle in state i to the time z, the corresponding physical situation could be the propagation of an electron-hole.

The lesser component is

$$G_{ij}^<(z, z') := \mp\frac{i}{\hbar}\Big\langle \hat{a}_j^\dagger(z')\hat{a}_i(z)\Big\rangle, \tag{2.18}$$

which first annihilates a particle in state i to the time z and at last creates a new particle in state j to the time z', the corresponding physical interpretation could be the propagation of a particle. These quantities for example describe the probability that certain states occur to the time z, after it was created to the time z'.
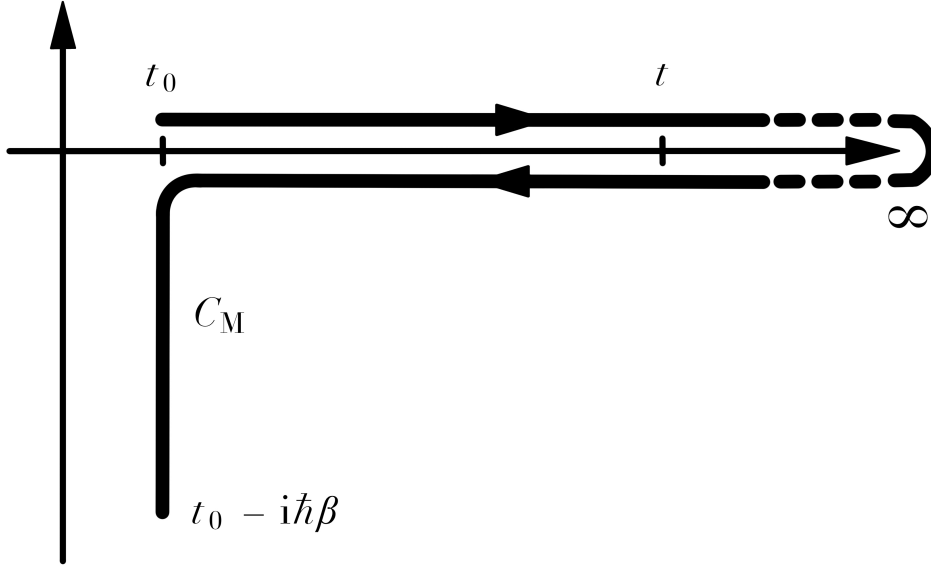

Figure 2.1: Schematic illustration of the Keldysh contour $\mathcal{C}$. It consist of a casual, an anti-casual branch and an imaginary branch which allows thermodynamic equilibrium correlations.[2][13]

2.2.1   Keldysh-Kadanoff-Baym Equation

To find the equation of motion for the 1pNEGF one needs to take the contour time derivative [14].

$$
i\hbar \frac{\partial}{\partial z} G_{ij}(z, z') = i\hbar \delta_{\mathcal{C}}(z - z') \big\{ G_{ij}^{>}(z, z') - G_{ij}^{<}(z, z') \big\}
$$
$$
+ \theta_{\mathcal{C}}(z - z') i\hbar \frac{\partial}{\partial z} G_{ij}^{>}(z, z') + \theta_{\mathcal{C}}(z' - z) i\hbar \frac{\partial}{\partial z} G_{ij}^{<}(z, z') \tag{2.19}
$$
$$
= \delta_{\mathcal{C}}(z - z') \delta_{ij} - \theta_{\mathcal{C}}(z - z') \Big\langle \frac{\partial \hat{a}_i(z)}{\partial z} \hat{a}_j^{\dagger}(z') \Big\rangle \mp \theta_{\mathcal{C}}(z' - z) \Big\langle \hat{a}_j^{\dagger}(z') \frac{\partial \hat{a}_i(z)}{\partial z} \Big\rangle \tag{2.20}
$$

The first term on the right-hand side of (2.19) is the contour time derivative of the contour theta function, which produces the contour delta function. The second and third term in (2.20) is the derivative of the annihilation operator with respect to contour time z, the

expression has already been found (2.14), we just need to substitute $t \to z$.
Thereby, the derivation results in:

$$
i\hbar\frac{\partial}{\partial z}G_{ij}(z,z') = \delta_{\mathcal{C}}(z-z')\delta_{ij} + \frac{i}{\hbar}\sum_{k}h_{ik}(z)\Big\{-\theta_{\mathcal{C}}(z-z')\big\langle\hat{a}_k(z)\hat{a}_j^\dagger(z')\big\rangle \mp \theta_{\mathcal{C}}(z'-z)\big\langle\hat{a}_j^\dagger(z')\hat{a}_k(z)\big\rangle\Big\}
$$
$$
-\frac{i}{\hbar}\sum_{mkl}\int_{\mathcal{C}}d\bar{z}\,w_{imkl}(z-z')
$$
$$
\times\Big\{\theta_{\mathcal{C}}(z-z')\big\langle\hat{a}_m^\dagger(\bar{z})\hat{a}_l(\bar{z})\hat{a}_k(z)\hat{a}_j^\dagger(z')\big\rangle \pm \theta_{\mathcal{C}}(z'-z)\big\langle\hat{a}_j^\dagger(z')\hat{a}_m^\dagger(\bar{z})\hat{a}_l(\bar{z})\hat{a}_k(z)\big\rangle\Big\}
$$
$$
\tag{2.21}
$$

$$
=\delta_{\mathcal{C}}(z-z')\delta_{ij} + \sum_{k}h_{ik}G_{kj}(z,z') - \frac{i}{\hbar}\sum_{mkl}\int_{\mathcal{C}}d\bar{z}\,w_{imkl}(z-z')
$$
$$
\times\Big\{\theta_{\mathcal{C}}(z-z')\big\langle\hat{a}_m^\dagger(\bar{z})\hat{a}_l(\bar{z})\hat{a}_k(z)\hat{a}_j^\dagger(z')\big\rangle \pm \theta_{\mathcal{C}}(z'-z)\big\langle\hat{a}_j^\dagger(z')\hat{a}_m^\dagger(\bar{z})\hat{a}_l(\bar{z})\hat{a}_k(z)\big\rangle\Big\}
$$
$$
\tag{2.22}
$$

with the equal time case $G_{ij}^>(z,z) - G_{ij}^<(z,z) = -\frac{i}{\hbar}\delta_{ij}$ and the second term of (2.22) $G_{ij}(z,z')$ being re-substituted. Further in (2.21) the two-time but instantaneous two particle interaction is defined $w(z-z') = \delta_{\mathcal{C}}(z-z')w$.
If the two-particle Green's function is identified

$$
G_{ijkl}^{(2)}(z,z';\bar{z},\bar{z}') = \left(-\frac{i}{\hbar}\right)^2\Big\langle\mathcal{T}_{\mathcal{C}}\big\{\hat{a}_i(z)\hat{a}_j(z')\hat{a}_l^\dagger(\bar{z}')\hat{a}_k^\dagger(\bar{z})\big\}\Big\rangle
\tag{2.23}
$$

in the expression above, we can write the simpler equation

$$
\sum_{k}\Big\{i\hbar\frac{\partial}{\partial z}\delta_{ik} - h_{ik}(z)\Big\}G_{kj}(z,z') = \delta_{\mathcal{C}}(z-z')\delta_{ij}
\tag{2.24}
$$
$$
\pm i\hbar\sum_{mkl}\int_{\mathcal{C}}d\bar{z}\,w_{imkl}(z-z')G_{lkjm}^{(2)}(z,\bar{z};z',\bar{z}^+).
\tag{2.25}
$$

Analogously, the adjoint KBE is derived, where the derivative was taken with respect to z' and (2.15) was used with $t \to z'$

$$
\sum_{k}G_{ik}(z,z')\Big\{-i\hbar\frac{\partial}{\partial z'}\delta_{kj} - h_{kj}(z')\Big\} = \delta_{\mathcal{C}}(z-z')\delta_{ij}
\tag{2.26}
$$
$$
\pm i\hbar\sum_{mkl}\int_{\mathcal{C}}d\bar{z}\,G_{likm}^{(2)}(z,\bar{z};z',\bar{z}^+)w_{kmjl}(z-z')
\tag{2.27}
$$

The 1pNEGF obeys an equation of motion, the Keldysh-Kadanoff-Baym equation (KBE) that is coupled to the higher order two-particle Green's function (2pNEGF). Further, the 2pNEGF obeys an own equation of motion and couples to the third particle Green's function

and so on. Thus, to solve the complete many-body problem the solution of the complete set of differential equations is needed, which scales exponentially with the number of particles like the TDSE. The whole set of equations is called the Martin-Schwinger Hierarchy[15]. Luckily, many-body perturbation theory allows to truncate the hierarchy and adequate approximations can be found. The collision term in the Keldysh-Kadanoff-Baym equation can be written with the self-energy $\Sigma_{ij}(z, \bar{z}) = \Sigma_{ij}[G, w](z, \bar{z})$, which is a functional of the one particle Green's function and the two particle interaction. Further, the way one wants to truncate the hierarchy defines the self-energy.

$$I_{ij}(z, z') = \pm i\hbar \sum_{mkl} \int_{\mathcal{C}} d\bar{z} \, w_{imkl}(z - z') G^{(2)}_{lkjm}(z, \bar{z}; z', \bar{z}^+) = \sum_{k} \int_{\mathcal{C}} d\bar{z} \, \Sigma_{ik}(z, \bar{z}) G_{kj}(\bar{z}, z') \quad (2.28)$$

and for the adjoint expression

$$\tilde{I}_{ij}(z, z') = \pm i\hbar \sum_{mkl} \int_{\mathcal{C}} d\bar{z} \, G^{(2)}_{likm}(z, \bar{z}; z', \bar{z}^+) w_{kmjl}(z - z') = \sum_{k} \int_{\mathcal{C}} d\bar{z} \, G_{ik}(z, \bar{z}) \Sigma_{kl}(\bar{z}, z') \quad (2.29)$$

The self-energy is an exact functional, which can not be computed. There are, however, systematic methods to construct good approximations[16].

2.2.2   Generalized Kadanoff-Baym Ansatz

To further reduce the computational effort the KBE the time diagonal limit of the 1pNEGF $\lim_{z, z' \to t} G^<_{ij}(z, z') = G^<_{ij}(t, t) =: G^<_{ij}(t)$ for $t \in \mathbb{R}$ is considered. One obtains the EOM with the derivative of the 1pNEGF with respect to time using (2.14) and (2.15):

$$i\hbar \frac{d}{dt} G^<_{ij}(t) - [h^{\mathrm{HF}}, G^<]_{ij}(t) = [I + I^\dagger]_{ij}(t) \quad (2.30)$$

with

$$h^{\mathrm{HF}}_{ij}(t) = h^{(0)}_{ij}(t) \pm i\hbar \sum_{kl} w^\pm_{ikjl}(t) G^<_{lk}(t). \quad (2.31)$$

Which is the effective one-body Hartree-Fock Hamiltonian as a sum of the non-interacting part $h^{(0)}_{ij}(t)$ and the Hartree-Fock mean-field contributions. We get these new terms when one substitutes

$$G^{(2),<}_{ijkl}(t) = G^{(2),\mathrm{H},<}_{ijkl}(t) \pm G^{(2),\mathrm{F},<}_{ijkl}(t) + G^{(2),\mathrm{corr}}_{ijkl}(t) = G^<_{ik}(t) G^<_{jl}(t) \pm G^<_{il}(t) G^<_{jk}(t) + \mathcal{G}_{ijkl}(t) \quad (2.32)$$

into the collision term.

The 2pNEGF can be written as a sum of Hartree and Fock Green's function and a correlation function, the Hartree-Fock terms are put into the commutator and the correlation Green's function is left in the collision term. The first two terms on the left accounts for uncorrelated joint probabilities for two bodies to be in certain states. The second term also takes into account the indistinguishability of particles with permuted indices, then the final term $G_{ijkl}^{(2),\mathrm{corr}}(t) =: \mathcal{G}_{ijkl}(t)$ accounts for correlation between two-particle states.

The collision term has the following structure:

$$I_{ij}(t) = \pm i\hbar \sum_{klm} w_{iklm}(t)\mathcal{G}_{lmjk}(t) = \sum_{k} \int_{t_0}^{t} d\bar{t} \left[\Sigma_{ik}^{>}(t,\bar{t})G_{kj}^{<}(\bar{t},t) - \Sigma_{ik}^{<}(t,\bar{t})G_{kj}^{>}(\bar{t},t) \right] \quad (2.33)$$

The off-diagonal elements of $G_{ij}^{\gtrless}(t,t')$ will be reconstructed with diagonal ones. In the exact case this yields a sum of integral and non integral terms. In practice, we neglect the integral term and approximate $G_{ij}^{\gtrless}(t,t')$ with the non integral ones. This procedure is called the Generalized Kadanoff-Baym Ansatz[17].

$$G_{ij}^{\gtrless}(t,t') \approx \pm \sum_{k} \left[G_{ik}^{\mathrm{R}}(t,t')n_{kj}^{\gtrless}(t') - n_{ik}^{\gtrless}(t)G_{kj}^{\mathrm{A}}(t,t') \right] = i\hbar \sum_{k} \left[G_{ik}^{\mathrm{R}}(t,t')G_{kj}^{\gtrless}(t') - G_{ik}^{\gtrless}(t)G_{kj}^{\mathrm{A}}(t,t') \right]$$

$$(2.34)$$

The one-particle reduced density matrix element $n_{ij}^{\gtrless}(t)$ can be identified and written as one particle Green's function. The retarded $G_{ij}^{\mathrm{R}}(t,t')$ and the advanced $G_{ij}^{\mathrm{A}}(t,t')$ Green's functions also obeys an similar complex EOM. To save computation time, the Hartree-Fock propagators are used.

$$G_{ij}^{\mathrm{R/A}}(t,t') = \mp \frac{i}{\hbar} \Theta\Big(\pm [t-t'] \Big) \exp\left(-\frac{i}{\hbar} \int_{t'}^{t} d\bar{t}\, h_{\mathrm{HF}}(\bar{t}) \right)\bigg|_{ij} \quad (2.35)$$

The structure of the right-hand side of equation (2.33) ensures non-linear time scaling, because of the memory integral, which means for every time step into the future, the collision term needs to integrate over all past times, thus all past events need to be considered.

2.3   G1–G2 Scheme

In this section a method to get linear time scaling will be presented, the G1–G2 scheme[1][2]. For this the GKBA needs to be reformulated by finding an own EOM for the correlation function $\mathcal{G}_{ijkl}(t)$, where two coupled differential equations for $G^{\gtrless}(t)$ and $\mathcal{G}(t)$ must be solved simultaneously. This reformulation gets rid of the memory integral and the result is an EOM that is local in time.

Therefore, with (2.34) we define for $t \geq t'$

$$G^{\gtrless}_{ij}(t' \leq t) = i\hbar \sum_k G^{\gtrless}_{ik}(t')\mathcal{U}_{kj}(t', t) \tag{2.36}$$

and for $t \leq t'$

$$G^{\gtrless}_{ij}(t \geq t') = i\hbar \sum_k \mathcal{U}_{ik}(t, t')G^{\gtrless}_{kj}(t') \tag{2.37}$$

in which the propagator $\mathcal{U}_{ij}(t, t')$ possesses properties of a time evolution operator for HF-GKBA

$$\mathcal{U}_{ij}(t, t') = G^{\mathrm{R}}_{ij}(t, t') - G^{\mathrm{A}}_{ij}(t, t'). \tag{2.38}$$

In order to find the coupled EOM the structure of the correlation function needs to be determined. For this reason, we introduce the self-energy used in all calculations in this thesis that accounts for correlated many-body effects up to second order:

$$\Sigma^{\mathrm{SOA},\gtrless}_{ij}(t, t') = \pm(i\hbar)^2 \sum_{klpqrs} w_{iklp}(t) w^{\pm}_{qrjs}(t') G^{\gtrless}_{lq}(t, t') G^{\gtrless}_{pr}(t, t') G^{\lessgtr}_{sk}(t', t), \tag{2.39}$$

with $w_{ijkl}(t) := w_{ijkl}(t) \pm w_{ijlk}(t)$ and plug it into (2.33). It will be used to determine the correlation function in terms of 1pNEGF. Hence, the comparison of the middle expression of (2.33) and the right-hand side of the same equation with plugged in $\Sigma^{\mathrm{SOA},\gtrless}_{ij}(t, t')$ yields

$$\mathcal{G}_{ijkl}(t) = (i\hbar)^3 \sum_{pqrs} \int_{t_0}^{t} d\bar{t}\, \mathcal{U}^{(2)}_{ijpq}(t, \bar{t}) \Psi^{\pm}_{pqrs}(\bar{t}) \mathcal{U}^{(2)}_{rskl}(\bar{t}, t). \tag{2.40}$$

The two-particle propagator is

$$\mathcal{U}^{(2)}_{ijkl}(t, t') = \mathcal{U}_{ik}(t, t')\mathcal{U}_{jl}(t, t') \tag{2.41}$$

where in the time-diagonal case

$$\mathcal{U}^{(2)}_{ijkl}(t,t) = \frac{1}{(i\hbar)^2}\delta_{ik}\delta_{jl}, \tag{2.42}$$

which is the product of two time-diagonal one-particle propagators.

$$\mathcal{U}_{ij}(t,t) = \frac{1}{i\hbar}\delta_{ij}. \tag{2.43}$$

The two-particle source term

$$\Psi^{\pm}_{ijkl}(t) = \frac{1}{(i\hbar)^2}\sum_{pqrs} w^{\pm}_{pqrs}(t)\Phi^{ijrs}_{pqkl}(t) \tag{2.44}$$

$$= (i\hbar)^2 \sum_{pqrs}\left(w_{pqrs}(t) \pm w_{pqsr}(t)\right)\left(G^{>}_{ip}(t)G^{>}_{jq}(t)G^{<}_{rk}(t)G^{<}_{sl}(t) - G^{<}_{ip}(t)G^{<}_{jq}(t)G^{>}_{rk}(t)G^{>}_{sl}(t)\right) \tag{2.45}$$

that accounts for pair correlation produced by two-particle scattering.

The next step is to differentiate the correlation function with respect to time in (2.40) using Leibniz integral rule.

$$\frac{d}{dt}\mathcal{G}_{ijkl}(t) = \left[\frac{d}{dt}\mathcal{G}_{ijkl}(t)\right]_{\int} + \left[\frac{d}{dt}\mathcal{G}_{ijkl}(t)\right]_{\mathcal{U}^{(2)}} \tag{2.46}$$

The derivatives will be divided up.

First, the derivative of the time-dependent two-particle propagator

$$\left[\frac{d}{dt}\mathcal{G}_{ijkl}(t)\right]_{\mathcal{U}^{(2)}} = (i\hbar)^3 \sum_{pqrs}\int_{t_0}^{t} d\bar{t}\,\Psi^{\pm}_{pqrs}(\bar{t})\left\{\left[\frac{\partial}{\partial t}\mathcal{U}^{(2)}_{ijpq}(t,\bar{t})\right]\mathcal{U}^{(2)}_{rskl}(\bar{t},t) + \mathcal{U}^{(2)}_{ijpq}(t,\bar{t})\left[\frac{\partial}{\partial t}\mathcal{U}^{(2)}_{rskl}(\bar{t},t)\right]\right\} \tag{2.47}$$

with

$$\frac{\partial}{\partial t}\mathcal{U}^{(2)}_{ijkl}(t,t') = \frac{1}{i\hbar}\sum_{pq} h^{(2),HF}_{ijpq}(t)\mathcal{U}^{(2)}_{pqkl}(t,t') \tag{2.48}$$

and

$$\frac{\partial}{\partial t}\mathcal{U}^{(2)}_{ijkl}(t',t) = -\frac{1}{i\hbar}\sum_{pq}\mathcal{U}^{(2)}_{ijpq}(t',t)h^{(2),HF}_{pqkl}(t), \tag{2.49}$$

where the two-particle Hartree-Fock Hamiltonian is defined as:

$$h_{ijkl}^{(2),\text{HF}}(t) = \delta_{jl}h_{ik}^{\text{HF}}(t) + \delta_{ik}h_{jl}^{\text{HF}}(t).\tag{2.50}$$

With this equation (2.47) becomes

$$\begin{aligned}
\left[\frac{d}{dt}\mathcal{G}_{ijkl}(t)\right]_{\mathcal{U}^{(2)}} =& (i\hbar)^3 \sum_{pqrs}\int_{t_0}^{t}d\bar{t}\,\Psi_{pqrs}^{\pm}(\bar{t}) \\
&\times \left\{\left[\frac{1}{i\hbar}\sum_{uv}h_{ijuv}^{(2),\text{HF}}(t)\mathcal{U}_{uvpq}^{(2)}(t,\bar{t})\right]\mathcal{U}_{rskl}^{(2)}(\bar{t},t) \right. \\
&\left. + \mathcal{U}_{ijpq}^{(2)}(t,\bar{t})\left[-\frac{1}{i\hbar}\sum_{uv}\mathcal{U}_{rsuv}^{(2)}(\bar{t},t)h_{uvkl}^{(2),\text{HF}}(t)\right]\right\}
\end{aligned}\tag{2.51}$$

, where the correlation function can be identified

$$\left[\frac{d}{dt}\mathcal{G}_{ijkl}(t)\right]_{\mathcal{U}^{(2)}} = \frac{1}{i\hbar}\sum_{pq}h_{ijpq}^{(2),\text{HF}}(t)\mathcal{G}_{pqkl}(t) - \frac{1}{i\hbar}\sum_{pq}\mathcal{G}_{ijpq}(t)h_{pqkl}^{(2),\text{HF}}(t)\tag{2.52}$$

and the second derivative, where the time dependence is in the limits.

$$\left[\frac{d}{dt}\mathcal{G}_{ijkl}(t)\right]_{\int} = (i\hbar)^3\sum_{pqrs}\mathcal{U}_{ijpq}^{(2)}(t,t)\Psi_{pqrs}^{\pm}(t)\mathcal{U}_{rskl}^{(2)}(t,t) = \frac{1}{i\hbar}\Psi_{ijkl}^{\pm}(t).\tag{2.53}$$

Finally, the sum of all time derivative contributions of $\mathcal{G}_{ijkl}(t)$ yields

$$i\hbar\frac{d}{dt}\mathcal{G}_{ijkl}(t) - [h^{(2),\text{HF}},\mathcal{G}]_{ijkl}(t) = \Psi_{ijkl}^{\pm}(t),\tag{2.54}$$

which couples to

$$i\hbar\frac{d}{dt}G_{ij}^{<}(t) - [h^{\text{HF}},G^{<}]_{ij}(t) = [I + I^{\dagger}]_{ij}(t)\tag{2.55}$$

through the collision term

$$I_{ij}(t) = \pm i\hbar\sum_{klp}w_{iklp}(t)\mathcal{G}_{lpjk}(t).\tag{2.56}$$

2.4 Introduction to Homogeneous Electron Gas

This subsection serves as a brief introduction to homogeneous electron gas (HEG) also known as Jellium. This model describes a system of electrons which are placed within a uniform background of positive charges. This means the ions are not localized on sites, instead on the contrary, they seem smeared out. If the lattice constant a of the ions is small in relation to the Fermi wavelength λ_{F} of the electrons, that means $\lambda_{\mathrm{F}} \gg a$, then to set $a = 0$ can be a good approximation. Thus, the uniform ion background can be justified and no lattice needs to be described. The Hamiltonian describing such a system will be presented in the following in first quantization. The Hamiltonian consists of electron-electron, the uniform background and the electron-background contributions.

$$\hat{H} = \hat{H}_{\mathrm{ee}} + \hat{H}_{\mathrm{backg}} + \hat{H}_{\mathrm{e\text{-}backg}} \tag{2.57}$$

First, the electron-electron Hamiltonian

$$\hat{H}_{\mathrm{ee}} = \sum_i \frac{\hat{\mathbf{p}}_i^2}{2m} + \frac{1}{2}e^2 \sum_{i \neq j} \frac{\mathrm{e}^{-\kappa|\mathbf{r}_i - \mathbf{r}_j|}}{|\mathbf{r}_i - \mathbf{r}_j|} \tag{2.58}$$

where the first term on the right-hand side is the kinetic energy. In the second term, the Yukawa potential was defined with κ being the inverse screening length.

The background contribution

$$\hat{H}_{\mathrm{backg}} = \frac{1}{2}e^2 \int d^3r' \int d^3r'' \, \rho(\mathbf{r}')\rho(\mathbf{r}'') \frac{\mathrm{e}^{-\kappa|\mathbf{r}' - \mathbf{r}''|}}{|\mathbf{r}' - \mathbf{r}''|} \tag{2.59}$$

$$= \frac{1}{2}e^2 \left(\frac{N}{V}\right)^2 \int d^3r' \int d^3r \, \frac{\mathrm{e}^{-\kappa|\mathbf{r}|}}{|\mathbf{r}|} = \frac{1}{2}e^2 \frac{N^2}{V} \frac{4\pi}{\kappa^2}, \tag{2.60}$$

with $\rho(\mathbf{r}) = \frac{N}{V}$ being the particle density and $\mathbf{r} := \mathbf{r}' - \mathbf{r}''$.

Finally, the electron-background contribute as follows:

$$\hat{H}_{\mathrm{e\text{-}backg}} = -e^2 \sum_i \int d^3r \, \rho(\mathbf{r}) \frac{\mathrm{e}^{-\kappa|\mathbf{r} - \mathbf{r}_i|}}{|\mathbf{r} - \mathbf{r}_i|} \tag{2.61}$$

$$= -e^2 \frac{N}{V} \sum_i^3 r \, \frac{\mathrm{e}^{-\kappa|\mathbf{r} - \mathbf{r}_i|}}{|\mathbf{r} - \mathbf{r}_i|} = -e^2 \frac{N^2}{V} \frac{4\pi}{\kappa^2}. \tag{2.62}$$

Therefore, the Hamiltonian in first quantization becomes

$$\hat{H} = \sum_i \frac{\hat{\mathbf{p}}_i^2}{2m} + \frac{1}{2}e^2 \sum_{i \neq j} \frac{\mathrm{e}^{-\kappa|\mathbf{r}_i - \mathbf{r}_j|}}{|\mathbf{r}_i - \mathbf{r}_j|} - \frac{1}{2}e^2 \frac{N^2}{V} \frac{4\pi}{\kappa^2}. \tag{2.63}$$

The jellium model is symmetric to translations, thus the appropriate basis is the plane-wave basis. Therefore, the transition for the Hamiltonian from the position representation to the momentum representation will be derived in the following. The formalism of second quantization is used [18]. First, the kinetic energy in the plane-wave basis takes a particularly simple form with the momentum eigenvalues $\langle \mathbf{k}_1 \sigma_1 | \mathbf{p} | \mathbf{k}_2 \sigma_2 \rangle = \hbar \mathbf{k} \delta_{\mathbf{k}_1, \mathbf{k}_2} \delta_{\sigma_1, \sigma_2}$.

$$\hat{H}^{\text{kin}} = \sum_i \frac{\hat{\mathbf{p}}_i^2}{2m} = \sum_{\mathbf{k}_1 \sigma_1} \frac{\hbar^2 \mathbf{k}_1^2}{2m} \hat{a}_{\mathbf{k}_1 \sigma_1}^\dagger \hat{a}_{\mathbf{k}_1 \sigma_1} \tag{2.64}$$

The interaction energy is

$$\hat{V} = \frac{1}{2} \sum_{\substack{\mathbf{k}_1 \mathbf{k}_2 \mathbf{k}_3 \mathbf{k}_4 \\ \sigma_1 \sigma_2 \sigma_3 \sigma_4}} \langle \mathbf{k}_1 \sigma_1 \mathbf{k}_2 \sigma_2 | \hat{V} | \mathbf{k}_3 \sigma_3 \mathbf{k}_4 \sigma_4 \rangle \hat{a}_{\mathbf{k}_1 \sigma_1}^\dagger \hat{a}_{\mathbf{k}_2 \sigma_2}^\dagger \hat{a}_{\mathbf{k}_4 \sigma_4} \hat{a}_{\mathbf{k}_3 \sigma_3}, \tag{2.65}$$

with

$$\langle \mathbf{k}_1 \sigma_1 \mathbf{k}_2 \sigma_2 | \hat{V} | \mathbf{k}_3 \sigma_3 \mathbf{k}_4 \sigma_4 \rangle = \int d^3 r' \int d^3 r'' \, V(\mathbf{r}', \mathbf{r}'') \langle \mathbf{k}_1 \sigma_1 | \mathbf{r}' \rangle \langle \mathbf{r}' | \mathbf{k}_3 \sigma_3 \rangle \langle \mathbf{k}_2 \sigma_2 | \mathbf{r}'' \rangle \langle \mathbf{r}'' | \mathbf{k}_4 \sigma_4 \rangle \tag{2.66}$$

$$= \frac{e^2}{V^2} \int d^3 r' \int d^3 r'' \frac{\mathrm{e}^{-\kappa |\mathbf{r}' - \mathbf{r}''|}}{|\mathbf{r}' - \mathbf{r}''|} \mathrm{e}^{-i\mathbf{k}_1 \cdot \mathbf{r}'} \mathrm{e}^{i\mathbf{k}_3 \cdot \mathbf{r}'} \mathrm{e}^{-i\mathbf{k}_2 \cdot \mathbf{r}''} \mathrm{e}^{i\mathbf{k}_4 \cdot \mathbf{r}''} \delta_{\sigma_1, \sigma_3} \delta_{\sigma_{12}, \sigma_4} \tag{2.67}$$

$$= \frac{e^2}{V^2} \delta_{\sigma_1, \sigma_3} \delta_{\sigma_2, \sigma_4} \int d^3 r \, \mathrm{e}^{-i(\mathbf{k}_1 + \mathbf{k}_2 - \mathbf{k}_3 - \mathbf{k}_4) \cdot \mathbf{r}} \int d^3 y \frac{\mathrm{e}^{-\kappa y}}{y} \mathrm{e}^{-i(\mathbf{k}_1 - \mathbf{k}_3) \cdot \mathbf{y}} \tag{2.68}$$

$$= \frac{e^2}{V} \delta_{\sigma_1, \sigma_3} \delta_{\sigma_2, \sigma_4} \delta_{\mathbf{k}_1 + \mathbf{k}_2, \mathbf{k}_3 + \mathbf{k}_4} \int d^3 y \frac{\mathrm{e}^{-\kappa y}}{y} \mathrm{e}^{-i(\mathbf{k}_1 - \mathbf{k}_3) \cdot \mathbf{y}} \tag{2.69}$$

$$= \frac{e^2}{V} \delta_{\sigma_1, \sigma_3} \delta_{\sigma_{12}, \sigma_4} \delta_{\mathbf{k}_1 + \mathbf{k}_2, \mathbf{k}_3 + \mathbf{k}_4} \frac{4\pi}{\mathbf{q}^2 + \kappa^2} \tag{2.70}$$

and $\langle \mathbf{k} | \mathbf{r} \rangle = \frac{\mathrm{e}^{-i\mathbf{k} \cdot \mathbf{r}}}{\sqrt{V}}$. That leads to the Hamilitonian in second quantization for the jellium model in momentum representation with $\kappa \to 0$.

$$\hat{H} = \sum_{\mathbf{k}_1 \sigma_1} \frac{\hbar^2 \mathbf{k}_1^2}{2m} \hat{a}_{\mathbf{k}_1 \sigma_1}^\dagger \hat{a}_{\mathbf{k}_1 \sigma_1} + \frac{e^2}{2V} \sum_{\substack{\mathbf{k}_1 \mathbf{k}_2 \mathbf{q} \\ \sigma_1 \sigma_2}} \frac{4\pi}{q^2} \hat{a}_{\mathbf{k}_1 + \mathbf{q} \sigma_1}^\dagger \hat{a}_{\mathbf{k}_2 - \mathbf{q} \sigma_2}^\dagger \hat{a}_{\mathbf{k}_2 \sigma_1} \hat{a}_{\mathbf{k}_1 \sigma_1}, \tag{2.71}$$

where the interaction matrix element is defined as $\frac{4\pi e^2}{|\mathbf{q}|^2} = v_{|\mathbf{q}|}$. A system that correspond to Jellium can be a conductor like a metal, in which the electrons are delocalized around the ions.

To extend HEG to the two-component case the Hamiltonian needs to be modified. Such that the second particle species, the ions are propagated on the same level as the electrons. The Hamiltonian can be split up into three parts.

$$\hat{H} = \hat{H}_{ee} + \hat{H}_{ii} + \hat{H}_{ei} \tag{2.72}$$

First, the Hamiltonian takes the electrons into account, it has the same structure as equation 2.71

$$\hat{H}_{ee} = \sum_{\mathbf{k},\sigma} \frac{\hbar^2 \mathbf{k}^2}{2m_e} \hat{a}_{\mathbf{k}\sigma}^\dagger \hat{a}_{\mathbf{k}\sigma} + \frac{1}{2V} \sum_{\mathbf{k}\mathbf{k}'\sigma\sigma'\mathbf{q}} v_{ee|\mathbf{q}|}(t) \hat{a}_{\mathbf{k}+\mathbf{q}\sigma}^\dagger \hat{a}_{\mathbf{k}'-\mathbf{q}\sigma'}^\dagger \hat{a}_{\mathbf{k}'\sigma'} \hat{a}_{\mathbf{k}\sigma}. \tag{2.73}$$

Then, the Hamiltonian that counts in ions is

$$\hat{H}_{ii} = \sum_{\mathbf{k},\sigma} \frac{\hbar^2 \mathbf{k}^2}{2m_i} \hat{b}_{\mathbf{k}\sigma}^\dagger \hat{b}_{\mathbf{k}\sigma} + \frac{1}{2V} \sum_{\mathbf{k}\mathbf{k}'\sigma\sigma'\mathbf{q}} v_{ii,|\mathbf{q}|}(t) \hat{b}_{\mathbf{k}+\mathbf{q}\sigma}^\dagger \hat{b}_{\mathbf{k}'-\mathbf{q}\sigma'}^\dagger \hat{b}_{\mathbf{k}'\sigma'} \hat{b}_{\mathbf{k}\sigma}, \tag{2.74}$$

where the matrix element for ion-ion interaction is $v_{ii,|\mathbf{q}|} = \frac{Z_i^2 4\pi e^2}{|\mathbf{q}|^2}$, with the charge number Z_i for arbitrary ion charge. At this point it should be noted that the charge number for electrons is $Z_e = 1$. Therefore, no charge number is explicitly presented on the right-hand side of equation 2.73.

Finally, the Hamiltonian that accounts for electron-ion interaction

$$\hat{H}_{ei} = \frac{1}{V} \sum_{\mathbf{k}\mathbf{k}'\sigma\sigma'\mathbf{q}} v_{ei,|\mathbf{q}|}(t) \hat{a}_{\mathbf{k}+\mathbf{q}\sigma}^\dagger \hat{b}_{\mathbf{k}'-\mathbf{q}\sigma'}^\dagger \hat{b}_{\mathbf{k}'\sigma'} \hat{a}_{\mathbf{k}\sigma}, \tag{2.75}$$

with the same modification for the matrix element as before $v_{ei,|\mathbf{q}|} = -\frac{Z_i 4\pi e^2}{|\mathbf{q}|^2}$. The only difference is the charge number of the electron $Z_e = 1$ is not explicitly written. Further, in equation 2.75, there is no factor one half, because no double-counting is considered. The negative sign emerge due to the fact that particles of different charges are taken into account. In general, ions can be fermions or bosons, it depends on the total spin number. To account for this fact creation and annihilation operators need to be defined for fermions and bosons differently, see section 2.1. Therefore, $\hat{a}$ ($\hat{a}^\dagger$) shall represent fermionic annihilation (creation) operator and $\hat{b}$ ($\hat{b}^\dagger$) for ions depending on the total spin number are either fermionic or bosonic annihilation (creation) operator. The generalization to a N-particle multi-component plasma is analogously. However, a simpler way to generalize multi-component plasma is to define a additional quantum number [4]. The particle species quantum number λ. Thus, the Hamiltonian becomes

$$\hat{H} = \sum_{\mathbf{k}\sigma\lambda} \frac{\hbar^2 \mathbf{k}^2}{2m_\lambda} \hat{a}_{\mathbf{k}\sigma}^{\dagger,\lambda} \hat{a}_{\mathbf{k}\sigma}^\lambda + \frac{1}{2V} \sum_{\mathbf{k}\mathbf{k}'\sigma\sigma'\mathbf{q}\lambda\lambda'} v_{|\mathbf{q}|}^{\lambda\lambda'}(t) \hat{a}_{\mathbf{k}+\mathbf{q}\sigma}^{\dagger,\lambda} \hat{a}_{\mathbf{k}'-\mathbf{q}\sigma'}^{\dagger,\lambda'} \hat{a}_{\mathbf{k}'\sigma'}^{\lambda'} \hat{a}_{\mathbf{k}\sigma}^\lambda, \tag{2.76}$$

with $\lambda = 1, 2, 3...N$ for N-particle species.

All properties of different particles are taken into account, with the particle species quantum number such as different masses, interaction potentials or if the creation and annihilation operators are fermionic or bosonic.

2.4.1   G1–G2: Transition into Momentum Representation

The plane momentum representation will be used, that leads for spatial homogenous systems to diagonality in the momentum, spin and species indices.

The transition from a general basis to the momentum basis for the G1–G2 scheme will be executed in the following paragraphs.

We begin with the 1pNEGF

$$G_{ij}(t) \to G_{\substack{\mathbf{k}_1 \mathbf{k}_1' \\ \alpha\alpha'}}^{\lambda\lambda'}(t) = G_{\substack{\mathbf{k}_1 \\ \alpha}}^{\lambda}(t)\delta_{\mathbf{k}_1,\mathbf{k}_1'}\delta_{\alpha,\alpha'}\delta_{\lambda,\lambda'}. \tag{2.77}$$

The indices $\mathbf{k}_1$, α and λ represent the momentum, spin and species respectively.

The δ's ensure that the 1pNEGF becomes diagonal because there is no one-particle process that changes the momentum, spin or species of a particle.

The interaction energy matrix element is

$$w_{ijkl}(t) \to w_{\substack{\mathbf{k}_1\mathbf{k}_2\mathbf{k}_3\mathbf{k}_4 \\ \alpha\beta\gamma\delta}}^{\lambda\mu\xi\eta}(t) = v_{\substack{\mathbf{k}_1,\mathbf{k}_2,\mathbf{k}_1-\mathbf{q},\mathbf{k}_2+\mathbf{q} \\ \alpha\beta\alpha\beta}}^{\lambda\mu\lambda\mu}(t)\delta_{\mathbf{k}_1+\mathbf{k}_2,\mathbf{k}_3+\mathbf{k}_4}\delta_{\alpha,\gamma}\delta_{\beta,\delta}\delta_{\lambda,\xi}\delta_{\mu,\eta} \tag{2.78}$$

$$=: v_{|\mathbf{k}_1-\mathbf{k}_3|}^{\lambda\mu}(t)\delta_{\mathbf{k}_1+\mathbf{k}_2,\mathbf{k}_3+\mathbf{k}_4}\delta_{\alpha,\gamma}\delta_{\beta,\delta}\delta_{\lambda,\xi}\delta_{\mu,\eta}, \tag{2.79}$$

where $\delta_{\mathbf{k}_1+\mathbf{k}_2,\mathbf{k}_3+\mathbf{k}_4}$ accounts for momentum conservation as expected from a translational invariant system and as before the diagonal nature of the interaction potential will be taken care of, with the remaining δ's to ensure no change in spin or particle species after collisions. There is just some transfer in momentum $\mathbf{k}_1 - \mathbf{k}_3 := \mathbf{q}$.

To the transition of the correlation function to the momentum basis, the structure of the 1pNEGF and the interaction matrix element leads to

$$\mathcal{G}_{ijkl}(t) \to \mathcal{G}_{\substack{\mathbf{k}_3\mathbf{k}_4\mathbf{k}_1\mathbf{k}_2 \\ \gamma\delta\alpha\beta}}^{\xi\eta\lambda\mu}(t) = \mathcal{G}_{\substack{\mathbf{k}_1-\mathbf{q},\mathbf{k}_2+\mathbf{q},\mathbf{k}_1,\mathbf{k}_2 \\ \alpha\beta\alpha\beta}}^{\lambda\mu\lambda\mu}(t)\delta_{\mathbf{k}_3+\mathbf{k}_4,\mathbf{k}_1+\mathbf{k}_2}\delta_{\alpha,\gamma}\delta_{\beta,\delta}\delta_{\lambda,\xi}\delta_{\mu,\eta} \tag{2.80}$$

$$=: \mathcal{G}_{\substack{\mathbf{k}_1\mathbf{k}_2\mathbf{q} \\ \alpha\beta}}^{\lambda\mu}(t)\delta_{\mathbf{k}_3+\mathbf{k}_4,\mathbf{k}_1+\mathbf{k}_2}\delta_{\alpha,\gamma}\delta_{\beta,\delta}\delta_{\lambda,\xi}\delta_{\mu,\eta}, \tag{2.81}$$

where $\delta_{\mathbf{k}_1+\mathbf{k}_2,\mathbf{k}_3+\mathbf{k}_4} = \delta_{\mathbf{q}+\mathbf{k}_2,\mathbf{k}_4}$ is used and the same considerations as before are made. Furthermore, equation (2.79) and (2.81) represent the reduced indices notation of the underlying

quantities that has the advantage of clearer representation and is easier to implement numerically. Then the EOM for $G'^{\lambda}_{\mathbf{k}_1 \atop \alpha}$ is

$$i\hbar \frac{d}{dt} G^{<,\lambda}_{\mathbf{k}_1 \atop \alpha}(t) = [I + I^{\dagger}]^{\lambda}_{\mathbf{k}_1 \atop \alpha}(t) + \underbrace{[h^{\mathrm{HF}}, G^{<}]^{\lambda}_{\mathbf{k}_1 \atop \alpha}(t)}_{=0} \tag{2.82}$$

$$= [I + I^{\dagger}]^{\lambda}_{\mathbf{k}_1 \atop \alpha}(t). \tag{2.83}$$

The one particle commutator vanishes because of the diagonal structure of the Hamiltonian and the 1pNEGF.

The reason will be shown in the following, first the Hartree-Fock Hamiltonian is evaluated

$$h^{\lambda\lambda',\mathrm{HF}}_{\mathbf{k}_1 \mathbf{k}'_1 \atop \alpha\alpha'}(t) = h^{\lambda\lambda',\mathrm{kin}}_{\mathbf{k}_1 \mathbf{k}'_1 \atop \alpha\alpha'}(t) + h^{\lambda\lambda',\mathrm{Hartree}}_{\mathbf{k}_1 \mathbf{k}'_1 \atop \alpha\alpha'}(t) + h^{\lambda\lambda',\mathrm{Fock}}_{\mathbf{k}_1 \mathbf{k}'_1 \atop \alpha\alpha'}(t). \tag{2.84}$$

The kinetic energy is

$$h^{\lambda\lambda',\mathrm{kin}}_{\mathbf{k}_1 \mathbf{k}'_1 \atop \alpha\alpha'}(t) = \frac{\hbar^2 \mathbf{k}_1^2}{2m_\lambda} \delta_{\mathbf{k}_1,\mathbf{k}'_1} \delta_{\alpha,\alpha'} \delta_{\lambda,\lambda'}, \tag{2.85}$$

which is the most trivial energy contribution in momentum space.

Then the Hartree energy

$$h^{\lambda\lambda',\mathrm{Hartree}}_{\mathbf{k}_1 \mathbf{k}'_1 \atop \alpha\alpha'}(t) = \pm i\hbar \sum_{\substack{\mathbf{k}_3 \mathbf{k}_4 \\ \gamma\delta \\ \xi\eta}} w^{\lambda\xi\lambda'\eta}_{\mathbf{k}_1 \mathbf{k}_3 \mathbf{k}'_1 \mathbf{k}_4 \atop \alpha\gamma\alpha'\delta}(t) G^{\eta\xi,<}_{\mathbf{k}_4 \mathbf{k}_3 \atop \delta\gamma}(t) \tag{2.86}$$

$$= \pm i\hbar \sum_{\substack{\mathbf{k}_4 \\ \delta \\ \eta}} v^{\lambda\eta}_{|0|}(t) G^{\eta,<}_{\mathbf{k}_4 \atop \delta}(t) \delta_{\mathbf{k}_1 \mathbf{k}'_1} \delta_{\alpha,\alpha'} \delta_{\lambda,\lambda'}, \tag{2.87}$$

where one needs to substitute the right-hand side of (2.77) and (2.79) into the first term of the Hartree Hamiltonian.

It is important to mention that the Hartree energy is divergent in a uniform system, but because a two-component system is considered, the divergent term will be compensated by the Hartree energy of oppositely charged particles. Still, the Hartree contribution will be neglected in the simulations because it is independent of momentum, therefore it provides

just a constant energy contribution and eventually does not contribute to any dynamics. The Fock energy is

$$
h^{\lambda\lambda',\text{Fock}}_{\substack{\mathbf{k}_1\mathbf{k}'_1\\\alpha\alpha'}}(t) = i\hbar \sum_{\substack{\mathbf{k}_3\mathbf{k}_4\\\gamma\delta\\\xi\eta}} w^{\lambda\xi\eta\lambda'}_{\substack{\mathbf{k}_1\mathbf{k}_3\mathbf{k}_4\mathbf{k}'_1\\\alpha\gamma\delta\alpha'}}(t) G^{\eta\xi,<}_{\substack{\mathbf{k}_4\mathbf{k}_3\\\delta\gamma}}(t) \tag{2.88}
$$

$$
= i\hbar \sum_{\mathbf{k}_4} v^{\lambda}_{|\mathbf{k}_1-\mathbf{k}_4|}(t) G^{\lambda,<}_{\substack{\mathbf{k}_4\\\alpha}}(t) \delta_{\mathbf{k}_1\mathbf{k}'_1} \delta_{\lambda,\lambda'} \delta_{\alpha,\alpha'} \tag{2.89}
$$

the same argumentation as before holds concerning the substitution of (2.77) and (2.79) into the first term of the Fock Hamiltonian.

Then the one-particle commutator vanishes

$$
[h^{\text{HF}}, G^{<}]^{\lambda}_{\substack{\mathbf{k}_1\\\alpha}}(t) = \sum_{k} h^{\lambda,\text{HF}}_{\substack{\mathbf{k}_1\mathbf{k}\\\alpha}}(t) G^{\lambda,<}_{\substack{\mathbf{k}\mathbf{k}_1\\\alpha}}(t) - G^{\lambda,<}_{\substack{\mathbf{k}_1\mathbf{k}\\\alpha}}(t) h^{\lambda,\text{HF}}_{\substack{\mathbf{k}\mathbf{k}_1\\\alpha}}(t) \tag{2.90}
$$

$$
= \left(h^{\lambda,\text{HF}}_{\substack{\mathbf{k}_1\\\alpha}}(t) G^{\lambda,<}_{\substack{\mathbf{k}_1\\\alpha}}(t) - G^{\lambda,<}_{\substack{\mathbf{k}_1\\\alpha}}(t) h^{\lambda,\text{HF}}_{\substack{\mathbf{k}_1\\\alpha}}(t) \right) \delta_{\mathbf{k}_1\mathbf{k}'_1} \delta_{\lambda,\lambda'} \delta_{\alpha,\alpha'} = 0. \tag{2.91}
$$

The dummy indices $k = (\mathbf{k}', \alpha', \lambda')$ contain the momentum spin and species indices, respectively.

Next, the collision integral will be evaluated with the help of (2.79) and (2.81).

$$
I^{\lambda\lambda'}_{\substack{\mathbf{k}_1\mathbf{k}'_1\\\alpha\alpha'}}(t) = \pm i\hbar \sum_{\substack{\mathbf{k}_2\mathbf{k}_3\mathbf{k}_4\\\beta\gamma\delta\\\mu\xi\eta}} w^{\lambda\mu\xi\eta}_{\substack{\mathbf{k}_1\mathbf{k}_2\mathbf{k}_3\mathbf{k}_4\\\alpha\beta\gamma\delta}}(t) \mathcal{G}^{\xi\eta\lambda'\mu}_{\substack{\mathbf{k}_3\mathbf{k}_4\mathbf{k}'_1\mathbf{k}_2\\\gamma\delta\alpha'\beta}}(t) \tag{2.92}
$$

$$
= \pm i\hbar \sum_{\substack{\mathbf{k}_2\mathbf{q}\\\beta\\\mu}} v^{\lambda\mu}_{|\mathbf{q}|}(t) \mathcal{G}^{\lambda\mu}_{\substack{\mathbf{k}_1\mathbf{k}_2\mathbf{q}\\\alpha\beta}}(t) \delta_{\mathbf{k}_1,\mathbf{k}'_1} \delta_{\alpha,\alpha'} \delta_{\lambda,\lambda'} \tag{2.93}
$$

and so the diagonal EOM for 1pNEGF is derived.

Next, the transition to the momentum representation of the EOM of the correlation function will be formulated.

$$
i\hbar \frac{d}{dt} \mathcal{G}^{\lambda\mu}_{\substack{\mathbf{k}_1\mathbf{k}_2\mathbf{q}\\\alpha\beta}}(t) - [h^{(2),\text{HF}}, \mathcal{G}]^{\lambda\mu}_{\substack{\mathbf{k}_1\mathbf{k}_2\mathbf{q}\\\alpha\beta}}(t) = \Psi^{\lambda\mu,\pm}_{\substack{\mathbf{k}_1\mathbf{k}_2\mathbf{q}\\\alpha\beta}}(t). \tag{2.94}
$$

For the two-particle commutator the full indices notation will be used to better understand the roles of the δ's.

$$
[h^{(2),\text{HF}}, \mathcal{G}]^{\lambda\mu\lambda\mu}_{\substack{\mathbf{k}_1-\mathbf{q},\mathbf{k}_2+\mathbf{q},\mathbf{k}_1,\mathbf{k}_2\\\alpha\beta\alpha\beta}}(t) = \sum_{mn} \left\{ h^{\lambda\mu,(2),\text{HF}}_{\substack{\mathbf{k}_1-\mathbf{q},\mathbf{k}_2+\mathbf{q},m,n\\\alpha\beta}}(t) \mathcal{G}^{\lambda\mu}_{\substack{m,n,\mathbf{k}_1,\mathbf{k}_2\\\alpha\beta}}(t) - \mathcal{G}^{\lambda\mu}_{\substack{\mathbf{k}_1-\mathbf{q},\mathbf{k}_2+\mathbf{q},m,n\\\alpha\beta}}(t) h^{\lambda\mu,(2),\text{HF}}_{\substack{m,n,\mathbf{k}_1,\mathbf{k}_2\\\alpha\beta}}(t) \right\}
$$

$$
\tag{2.95}
$$

The dummy indices $m = (\mathbf{k}', \alpha', \lambda')$ and $n = (\mathbf{k}'', \alpha'', \lambda'')$ contain the momentum, spin and species indices, respectively.

The two-particle Hamiltonian in the two-particle commutator will be evaluated separately and takes the following form.

$$h^{\lambda\mu,(2),\mathrm{HF}}_{\substack{\mathbf{k}_1-\mathbf{q},\mathbf{k}_2+\mathbf{q},m,n \\ \alpha\beta}}(t) = \delta_{\mathbf{k}_2+\mathbf{q},n}\, h^{\lambda,\mathrm{HF}}_{\substack{\mathbf{k}_1-\mathbf{q},m \\ \alpha}}(t) + \delta_{\mathbf{k}_1-\mathbf{q},m}\, h^{\mu,\mathrm{HF}}_{\substack{\mathbf{k}_2+\mathbf{q},n \\ \beta}}(t) \tag{2.96}$$

$$\tag{2.97}$$

and

$$h^{\lambda\mu,(2),HF}_{\substack{m,n,\mathbf{k}_1,\mathbf{k}_2 \\ \alpha\beta}}(t) = \delta_{n,\mathbf{k}_2}\, h^{\lambda,HF}_{\substack{m,\mathbf{k}_1 \\ \alpha}}(t) + \delta_{m,\mathbf{k}_1}\, h^{\mu,HF}_{\substack{n,\mathbf{k}_2 \\ \beta}}(t). \tag{2.98}$$

Then the commutator parts can be evaluated. The first term is

$$\sum_{mn} h^{\lambda\mu,(2),HF}_{\substack{\mathbf{k}_1-\mathbf{q},\mathbf{k}_2+\mathbf{q},m,n \\ \alpha\beta}}(t)\, \mathcal{G}^{\lambda\mu}_{\substack{m,n,\mathbf{k}_1,\mathbf{k}_2 \\ \alpha\beta}}(t) = \sum_{mn}\{\delta_{\mathbf{k}_2+\mathbf{q},n}\, h^{\lambda,HF}_{\substack{\mathbf{k}_1-\mathbf{q},m \\ \alpha}}(t)\mathcal{G}^{\lambda\mu}_{\substack{m,n,\mathbf{k}_1,\mathbf{k}_2 \\ \alpha\beta}}(t) + \delta_{\mathbf{k}_1-\mathbf{q},m}\, h^{\mu,HF}_{\substack{\mathbf{k}_2+\mathbf{q},n \\ \beta}}(t)\mathcal{G}^{\lambda\mu}_{\substack{m,n,\mathbf{k}_1,\mathbf{k}_2 \\ \alpha\beta}}(t)\} \tag{2.99}$$

$$= \sum_{mn}\{h^{\lambda,HF}_{\substack{\mathbf{k}_1-\mathbf{q} \\ \alpha}}(t)\mathcal{G}^{\lambda\mu}_{\substack{m,n,\mathbf{k}_1,\mathbf{k}_2 \\ \alpha\beta}}(t) + h^{\mu,HF}_{\substack{\mathbf{k}_2+\mathbf{q} \\ \beta}}(t)\mathcal{G}^{\lambda\mu}_{\substack{m,n,\mathbf{k}_1,\mathbf{k}_2 \\ \alpha\beta}}(t)\}\delta_{\mathbf{k}_2+\mathbf{q},n}\delta_{\mathbf{k}_1-\mathbf{q},m} \tag{2.100}$$

$$= h^{\lambda,HF}_{\substack{\mathbf{k}_1-\mathbf{q} \\ \alpha}}(t)\mathcal{G}^{\lambda\mu\lambda\mu}_{\substack{\mathbf{k}_1-\mathbf{q},\mathbf{k}_2+\mathbf{q},\mathbf{k}_1,\mathbf{k}_2 \\ \alpha\beta\alpha\beta}}(t) + h^{\mu,HF}_{\substack{\mathbf{k}_2+\mathbf{q} \\ \beta}}(t)\mathcal{G}^{\lambda\mu\lambda\mu}_{\substack{\mathbf{k}_1-\mathbf{q},\mathbf{k}_2+\mathbf{q},\mathbf{k}_1,\mathbf{k}_2 \\ \alpha\beta\alpha\beta}}(t) \tag{2.101}$$

and the second term is

$$\sum_{mn} \mathcal{G}^{\lambda\mu}_{\substack{\mathbf{k}_1-\mathbf{q},\mathbf{k}_2+\mathbf{q},m,n \\ \alpha\beta}}(t)\, h^{\lambda\mu,(2),HF}_{\substack{m,n,\mathbf{k}_1,\mathbf{k}_2 \\ \alpha\beta}}(t) = \sum_{mn}\{\delta_{n,\mathbf{k}_2}\mathcal{G}^{\lambda\mu}_{\substack{\mathbf{k}_1-\mathbf{q},\mathbf{k}_2+\mathbf{q},m,n \\ \alpha\beta}}(t)h^{\lambda,HF}_{\substack{m,\mathbf{k}_1 \\ \alpha}}(t) + \delta_{m,\mathbf{k}_1}\mathcal{G}^{\lambda\mu}_{\substack{\mathbf{k}_1-\mathbf{q},\mathbf{k}_2+\mathbf{q},m,n \\ \alpha\beta}}(t)h^{\mu,HF}_{\substack{n,\mathbf{k}_2 \\ \beta}}(t)\} \tag{2.102}$$

$$= \sum_{mn}\{\mathcal{G}^{\lambda\mu}_{\substack{\mathbf{k}_1-\mathbf{q},\mathbf{k}_2+\mathbf{q},m,n \\ \alpha\beta}}(t)h^{\lambda,HF}_{\substack{\mathbf{k}_1 \\ \alpha}}(t) + \mathcal{G}^{\lambda\mu}_{\substack{\mathbf{k}_1-\mathbf{q},\mathbf{k}_2+\mathbf{q},m,n \\ \alpha\beta}}(t)h^{\mu,HF}_{\substack{\mathbf{k}_2 \\ \beta}}(t)\}\delta_{n,\mathbf{k}_2}\delta_{m,\mathbf{k}_1} \tag{2.103}$$

$$= \mathcal{G}^{\lambda\mu\lambda\mu}_{\substack{\mathbf{k}_1-\mathbf{q},\mathbf{k}_2+\mathbf{q},\mathbf{k}_1,\mathbf{k}_2 \\ \alpha\beta\alpha\beta}}(t)h^{\lambda,HF}_{\substack{\mathbf{k}_1 \\ \alpha}}(t) + \mathcal{G}^{\lambda\mu\lambda\mu}_{\substack{\mathbf{k}_1-\mathbf{q},\mathbf{k}_2+\mathbf{q},\mathbf{k}_1,\mathbf{k}_2 \\ \alpha\beta\alpha\beta}}(t)h^{\mu,HF}_{\substack{\mathbf{k}_2 \\ \beta}}(t) \tag{2.104}$$

It can be seen that because of the diagonality of the Hartree-Fock Hamiltonian shown before, second δ's arise and modify the terms.

So, equation (2.95) becomes in reduced index notation

$$[h^{(2),HF},\mathcal{G}]^{\lambda\mu}_{\substack{\mathbf{k}_1\mathbf{k}_2\mathbf{q} \\ \alpha\beta}}(t) = \Big\{h^{\lambda,HF}_{\substack{\mathbf{k}_1-\mathbf{q} \\ \alpha}}(t) + h^{\mu,HF}_{\substack{\mathbf{k}_2+\mathbf{q} \\ \beta}}(t) - h^{\lambda,HF}_{\substack{\mathbf{k}_1 \\ \alpha}}(t) - h^{\mu,HF}_{\substack{\mathbf{k}_2 \\ \beta}}(t)\Big\}\mathcal{G}^{\lambda\mu}_{\substack{\mathbf{k}_1\mathbf{k}_2\mathbf{q} \\ \alpha\beta}}(t). \tag{2.105}$$

The next and final expression, so we can explicitly formulate the EOM of the correlation function, is the two particle source term in full indices notation in momentum representation.

$$\Psi^{\lambda\mu\lambda\mu,\pm}_{\substack{\mathbf{k}_1-\mathbf{q},\mathbf{k}_2+\mathbf{q},\mathbf{k}_1,\mathbf{k}_2\\ \alpha\beta\alpha\beta}}(t) = \frac{1}{(i\hbar)^2}\sum_{pqrs}w^{\pm}_{pqrs}(t)\Phi^{\mathbf{k}_1-\mathbf{q},\mathbf{k}_2+\mathbf{q},r,s}_{p,q,\mathbf{k}_1,\mathbf{k}_2}(t) \tag{2.106}$$

$$= \frac{1}{(i\hbar)^2}\sum_{pqrs}(w_{pqrs}(t)\pm w_{pqsr}(t))(i\hbar)^4(G^{\lambda,>}_{\substack{\mathbf{k}_1-\mathbf{q},p\\\alpha}}(t)G^{\mu,>}_{\substack{\mathbf{k}_2+\mathbf{q},q\\\beta}}(t)G^{\lambda,<}_{\substack{r,\mathbf{k}_1\\\alpha}}(t)G^{\mu,<}_{\substack{s,\mathbf{k}_2\\\beta}}(t) - (>\leftrightarrow<)) \tag{2.107}$$

$$= (i\hbar)^2\sum_{pqrs}(w_{pqrs}(t)\pm w_{pqsr}(t))(G^{\lambda,>}_{\substack{\mathbf{k}_1-\mathbf{q}\\\alpha}}(t)G^{\mu,>}_{\substack{\mathbf{k}_2+\mathbf{q}\\\beta}}(t)G^{\lambda,<}_{\substack{\mathbf{k}_1\\\alpha}}(t)G^{\mu,<}_{\substack{\mathbf{k}_2\\\beta}}(t)\delta_{\mathbf{k}_1-\mathbf{q},p}\delta_{\mathbf{k}_2+\mathbf{q},q}\delta_{r,\mathbf{k}_1}\delta_{s,\mathbf{k}_2} - (>\leftrightarrow<)) \tag{2.108}$$

$$= (i\hbar)^2(w^{\lambda\mu\lambda\mu}_{\substack{\mathbf{k}_1-\mathbf{q},\mathbf{k}_2+\mathbf{q},\mathbf{k}_1,\mathbf{k}_2\\\alpha\beta\alpha\beta}}(t)\pm w^{\lambda\mu\mu\lambda}_{\substack{\mathbf{k}_1-\mathbf{q},\mathbf{k}_2+\mathbf{q},\mathbf{k}_2,\mathbf{k}_1\\\alpha\beta\beta\alpha}}(t))(G^{\lambda,>}_{\substack{\mathbf{k}_1-\mathbf{q}\\\alpha}}(t)G^{\mu,>}_{\substack{\mathbf{k}_2+\mathbf{q}\\\beta}}(t)G^{\lambda,<}_{\substack{\mathbf{k}_1\\\alpha}}(t)G^{\mu,<}_{\substack{\mathbf{k}_2\\\beta}}(t) - (>\leftrightarrow<)) \tag{2.109}$$

$$= (i\hbar)^2(v^{\lambda\mu}_{|\mathbf{q}|}(t)\pm v^{\lambda\lambda}_{|\mathbf{k}_1-\mathbf{q}-\mathbf{k}_2|}(t)\delta_{\alpha,\beta}\delta_{\lambda\mu})(G^{\lambda,>}_{\substack{\mathbf{k}_1-\mathbf{q}\\\alpha}}(t)G^{\mu,>}_{\substack{\mathbf{k}_2+\mathbf{q}\\\beta}}(t)G^{\lambda,<}_{\substack{\mathbf{k}_1\\\alpha}}(t)G^{\mu,<}_{\substack{\mathbf{k}_2\\\beta}}(t) - (>\leftrightarrow<)), \tag{2.110}$$

again with dummy indices $p = (\mathbf{k}', \alpha', \lambda')$, $q = (\mathbf{k}'', \alpha'', \lambda'')$, $r = (\mathbf{k}''', \alpha''', \lambda''')$ and $s = (\mathbf{k}'''', \alpha'''', \lambda'''')$. It can be noticed on the fifth expression, on right-hand side that the SOA-exchange term only shows up for identical particles. With this, the transition of the G1–G2 scheme from a general basis into momentum base is completed. It should be pointed out that the quantities in this section are formulated for a discrete momentum basis, just like the simulation can only sample a discrete momentum spectrum, but in fact the system is considered continuous. That means, the following substitution must be made

$$\sum_{\mathbf{k}} \to \int \frac{dk^n}{(2\pi\hbar)^n} \tag{2.111}$$

and

$$G^{<,\lambda}_{\substack{\mathbf{k}\\\alpha}}(t) = \mp\frac{i}{\hbar}\langle \hat{a}^{\dagger,\lambda}_{\substack{\mathbf{k}\\\alpha}}(t)\hat{a}^{\lambda}_{\substack{\mathbf{k}\\\alpha}}(t)\rangle \to G^{<,\lambda}_{\alpha}(\mathbf{k},t) = \mp\frac{i}{\hbar}\langle \hat{\Psi}^{\dagger,\lambda}_{\alpha}(\mathbf{k},t)\hat{\Psi}^{\lambda}_{\alpha}(\mathbf{k},t)\rangle \tag{2.112}$$

The field operators $\hat{\Psi}^{\dagger}(\mathbf{k},t)$ and $\hat{\Psi}(\mathbf{k},t)$ are the continuous generalization of the creation and annihilation operator, which obey the same commutator relation with the substitution $\delta_{i,j} \to \delta(i-j)$.

2.5   Observables in the G1–G2 scheme

In this section observables are presented, that can be obtained from the 1pNEGF in the general as well as in the momentum representation.

The one-particle reduced density matrix (1pRDM) that gives the probability for certain states to be occupied:

$$n_{ij} = \langle \hat{a}_j^\dagger(t)\hat{a}_i(t)\rangle \tag{2.113}$$

and the momentum representation

$$n_{\mathbf{k}_1\atop\alpha}^\lambda(t) = \langle \hat{a}_{\mathbf{k}_1\atop\alpha}^{\dagger,\lambda}(t)\hat{a}_{\mathbf{k}_1\atop\alpha}^\lambda(t)\rangle. \tag{2.114}$$

Because of the diagonal structure of the NEGF the one particle density matrix takes a particularly simple form. The relation from the 1pRDM to the lesser component of the Green's function is presented with the following relation

$$G_{ij}^<(t) = \pm\frac{1}{i\hbar}n_{ij}(t) = G_{ij}^>(t) - \frac{1}{i\hbar}\delta_{ij} \tag{2.115}$$

with the momentum representation

$$G_{\mathbf{k}_1\atop\alpha}^{<,\lambda}(t) = \pm\frac{1}{i\hbar}n_{\mathbf{k}_1\atop\alpha}^\lambda(t) = G_{\mathbf{k}_1\atop\alpha}^{>,\lambda}(t) - \frac{1}{i\hbar}. \tag{2.116}$$

The kinetic energy matrix element is

$$h_{ij}^{\text{kin}} = \frac{\mathbf{p}_{ij}^2}{2m} \tag{2.117}$$

in momentum representation the kinetic energy is

$$h_{\mathbf{k}_1\atop\alpha}^{\lambda,\text{kin}} = \frac{\hbar^2\mathbf{k}_1^2}{2m_\lambda}. \tag{2.118}$$

The Hartree energy matrix element is

$$h_{ij}^{\text{Hartree}}(t) = \pm i\hbar\sum_{kl} w_{ikjl}(t)G_{lk}^<(t) \tag{2.119}$$

and the divergent momentum representation

$$h_{\mathbf{k}_1 \atop \alpha}^{\lambda,\text{Hartree}}(t) = \pm i\hbar \sum_{\mathbf{k}_4 \atop {\delta \atop \eta}} v_{|0|}^{\lambda\eta}(t) G_{\mathbf{k}_4 \atop \delta}^{\eta,<}(t). \tag{2.120}$$

The Fock energy is

$$h_{ij}^{\text{Fock}}(t) = i\hbar \sum_{kl} w_{iklj}(t) G_{lk}^{<}(t) \tag{2.121}$$

and the Fock energy matrix element in momentum representation

$$h_{\mathbf{k}_1 \atop \alpha}^{\lambda,\text{Fock}}(t) = i\hbar \sum_{\mathbf{k}_4} v_{|\mathbf{k}_1 - \mathbf{k}_4|}^{\lambda}(t) G_{\mathbf{k}_4 \atop \alpha}^{\lambda,<}(t) \tag{2.122}$$

further is noted, because of the diagonal nature of the momentum representation, the one-particle energy matrix elements are energy eigenvalues.

The time-dependent expectation values of the Hamiltonian can be formulated.

$$\langle \hat{H} \rangle(t) = \langle \hat{H}^{\text{kin}} \rangle(t) + \langle \hat{H}^{\text{HF}} \rangle(t) + \langle \hat{H}^{\text{corr}} \rangle(t), \tag{2.123}$$

with $\langle \hat{H}^{\text{int}} \rangle(t) = \langle \hat{H}^{\text{HF}} \rangle(t) + \langle \hat{H}^{\text{corr}} \rangle(t)$.

The expectation value of the kinetic energy is

$$\langle \hat{H}^{\text{kin}} \rangle(t) = Tr\left(H^{\text{kin}} n(t)\right), \tag{2.124}$$

where the expectation value is just the trace over the product of the kinetic energy and the 1pRDM. The same is valid for the other terms. The expectation value of the interaction energy can be split in a mean-field part

$$\langle \hat{H}^{\text{HF}} \rangle(t) = \frac{1}{2} Tr\left(H^{\text{HF}}(t) n(t)\right) \tag{2.125}$$

and the correlated part

$$\langle \hat{H}^{\text{corr}} \rangle(t) = \frac{1}{2} \mathfrak{Im}\left\{ Tr\left(I(t)\right) \right\}, \tag{2.126}$$

with the imaginary part of the trace over the collision integral. Furthermore, since the momentum also is a important quantity in the plasma, the expectation value of the momentum operator is expressed.

$$\langle \hat{\mathbf{p}} \rangle(t) = Tr\Big(\mathbf{p} n(t)\Big) \tag{2.127}$$

It should be noted that the abstract operator notation is independent of representations.

3 Setup

In this section some simulation related aspects will be presented.

The simulation was written by Christopher Makait for a one-dimensional quantum wire with spatially homogeneously distributed electrons, a jellium plasma described with the G1–G2 scheme. I expanded the jellium program by a second particle species, the positive charged ions of arbitrary mass. Additionally, a particle beam was implemented belonging to one of the two mentioned species respectively. The system described is spin symmetrical, that means there is no different behavior between particles with spin up or spin down.

The properties of the confined particles in the wire are as follows, in longitudinal direction the particles behave free and in radial direction the particles are confined in the harmonic potential

$$v(r_\perp) = \frac{1}{2}m\omega^2 r_\perp^2. \tag{3.1}$$
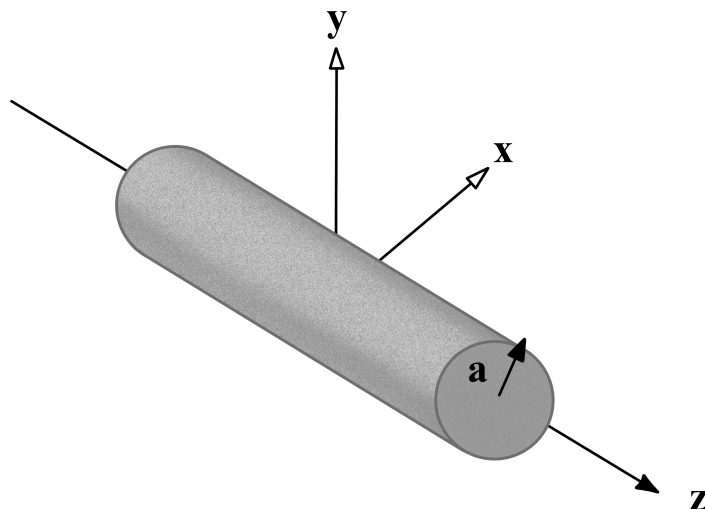
Figure 3.1: Illustration of the one-dimensional quantum wire, with radius a.[19][13]

The excited states are not strongly occupied for large ω, thus all excited states are neglected.

The wave function in ground state is of the form

$$\phi_0(r_\perp) = \left(\frac{2}{\pi a^2}\right)^{\frac{1}{2}} e^{-r_\perp^2/a^2}, \tag{3.2}$$

this can be used to calculate the Yukawa matrix elements $\langle \mathbf{k}_1'\alpha'\lambda', \mathbf{k}_2'\beta'\mu' \mid e^2 \dfrac{e^{-\kappa r}}{r} \mid \mathbf{k}_1\alpha\lambda, \mathbf{k}_2\beta\mu \rangle$, with $\langle \mathbf{r}\sigma'\lambda' \mid \mathbf{k}\sigma\lambda \rangle \equiv \phi_0(r_\perp)\dfrac{e^{i\mathbf{k}\cdot\mathbf{r}_\parallel}}{\sqrt{L}}\delta_{\sigma'\sigma}\delta_{\lambda'\lambda}$.

Which yield

$$v(q_\parallel) = -e^2 \exp\left((q_\parallel^2 + \kappa^2)a^2\right)\mathrm{Ei}(-(q_\parallel^2 + \kappa^2)a^2), \tag{3.3}$$

with $k_{1,\parallel} - k_{2,\parallel} := q_\parallel$, the wire radius a, the inverse screening length κ, the elementary charge e and finally the exponential integral Ei. The detailed derivation can be found in [19].
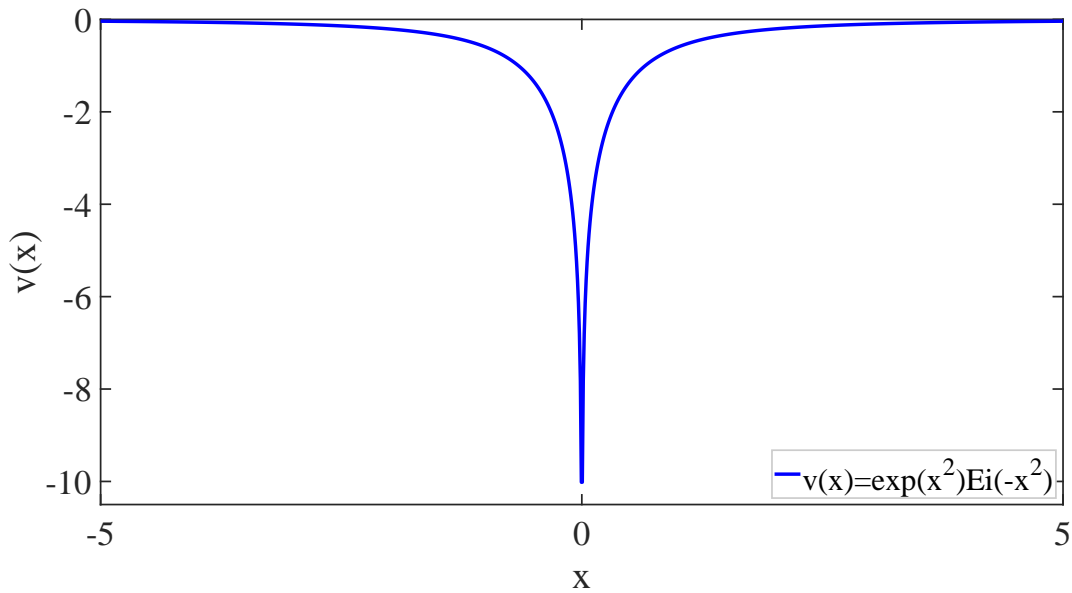
Figure 3.2: Interaction energy

Another important aspect is to select the initial state of the 1pNEGF $G_0^<(t_0) = \pm\dfrac{1}{i\hbar}n_0(t_0)$, which represents the occupation number at the beginning of the propagation at time t_0. For this, the simulation has three different initialisation modes. The first one consist of two shifted gaussian type distributions, the second one is the Fermi-Dirac distribution, which just takes the kinetic energy into account. The third one initializes with a Fermi distribution but on Hartree-Fock level, which in contrast to the ordinary Fermi-distribution also includes

the Hartree-Fock energy self-consistently at the beginning.

Throughout this thesis all calculations are initialized on the third initialization mode.

$$G_{\substack{k \\ \alpha}}^{<,\lambda}(t_0) = \pm \frac{1}{i\hbar} \frac{1}{\exp\left(\frac{h_k^{\mathrm{HF},\lambda}(t_0)-\mu}{k_B T^\lambda}\right) + 1} \tag{3.4}$$

The particle beam is added with a Gaussian distribution at time t_0 to a specific particle momentum distribution.

$$\tilde{G}_0^{<,\lambda}(t_0) := G_0^{<,\lambda}(t_0) + G_{\mathrm{beam}}^<(t_0), \tag{3.5}$$

with the matrix elements for the beam distribution

$$G_{\substack{\mathrm{beam},k \\ \alpha}}^{<,\lambda}(t_0) = \pm \frac{1}{i\hbar} A \exp\left(-\frac{1}{2}\left(\frac{k-k_0}{\sigma}\right)^2\right), \tag{3.6}$$

where A is the amplitude, k_0 is the peak position and σ is the width of the beam.

The charge neutrality of the two species in the bulk system is ensured with the constraint

$$\sum_{\mathbf{k}\sigma\lambda} q^\lambda G_{\substack{\mathbf{k} \\ \alpha}}^{<,\lambda}(t_0) = 0. \tag{3.7}$$

However, the interaction of the two bulks are not investigated in this thesis, just interaction between bulk and beam. In this setup there is no charge neutrality, nevertheless it is a feature of the program.

In the following a resume of the most important parameters of the simulations is presented.

- `NKR`: The number of grid points that are sampled on the momentum axis.

- `CUTOFFMOMENTUM`: The region that is sampled, everything outside the interval is not computed.

- `DT`: Witdh of time steps.

- `KAPPAFACTOR`: The inverse screening length of the potential.

- `PROPT`: Maximum number of time steps.

- `RADIUS`: Radius of the wire in Bohr radii.

- `DENSITY`: Particle number per Bohr radius.

- `BETA`: Is the thermodynamic beta of electrons.

- `THETA`: The ratio of the thermal energy and the Fermi energy (alternative to `BETA`)

- `BETA_ION_1`: Is the thermodynamic beta of ions.

- `MU`: Is the chemical potential of electrons.

- `MU_ION_1`: Is the chemical potential of ions.

- `MASSE_ION_1`: Mass of ions.

It is worth mentioning, that parameters for adiabatic switching exist, that are not used throughout this thesis, because the initial distribution needs too much time to thermalize. Furthermore, the SOA exchange term in the two-particle source term was neglected because there were barely any differences seen in the simulation. The simulation was parallelized with OpenMP, but because of the rapid saturation with the core number and the high serial ratio with Eigen operations, barely any acceleration was observed, see figure 3.3.
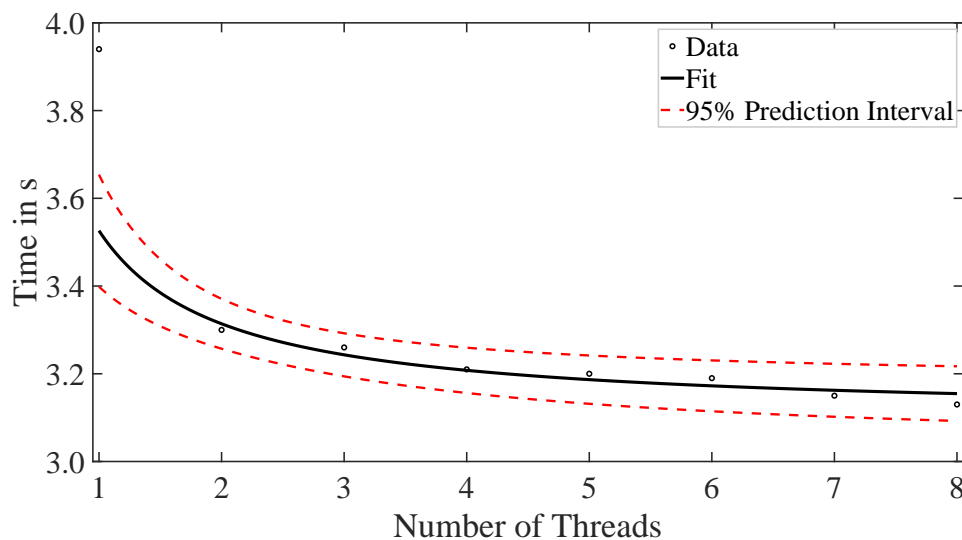
Figure 3.3: Computation time for `NKR` = 200 for every time step for different thread numbers.

Further Hartree atomic units were used where we set the reduced Planck constant to $\hbar = 1$, the elementary charge to $e = 1$, the Bohr radius to $a_0 = 1$ and finally the electron mass to $m_e = 1$. To better interpret the magnitude of the most important physical quantities used in this thesis, the conversion from atomic units to SI will be presented:

- Energy:

$$E_{\text{SI}} = \frac{\hbar^2}{m_e a_0^2} \times E_{\text{a.u.}} \approx 4.36 \times 10^{-18}\,\text{J} \times E_{\text{a.u.}} \tag{3.8}$$

■ Time:

$$t_{\text{SI}} = \frac{m_e a_0^2}{\hbar} \times t_{\text{a.u.}} \approx 2.42 \times 10^{-17}\,\text{s} \times t_{\text{a.u.}} \tag{3.9}$$

■ Momentum:

$$p_{\text{SI}} = \frac{\hbar}{a_0} \times p_{\text{a.u.}} \approx 1.99 \times 10^{-24}\,\text{kg}\,\text{m}\,\text{s}^{-1} \times p_{\text{a.u.}} \tag{3.10}$$

■ Temperature:

$$T_{\text{SI}} = \frac{\hbar^2}{m_e a_0^2 k_B} \times \beta_{\text{a.u.}}^{-1} \approx 3.16 \times 10^5\,\text{K} \times \beta_{\text{a.u.}}^{-1} \tag{3.11}$$

■ Density:

$$n_{\text{SI}} = \frac{1}{a_0} \times n_{\text{a.u.}} \approx 1.89 \times 10^{10}\,\text{m}^{-1} \times n_{\text{a.u.}} \tag{3.12}$$

■ Radius:

$$r_{\text{SI}} = a_0 \times r_{\text{a.u.}} \approx 5.29 \times 10^{11}\,\text{m} \times r_{\text{a.u.}} \tag{3.13}$$

The time propagation of all relevant quantities is made with the fourth-order Runge-Kutta stepper and the code is written with the programming language C++. All results presented in this thesis are computed with a High Performance Computer at the Linux-Cluster of the University Computing Centre at Christian-Albrechts-Universität zu Kiel.

3.1   Convergence

The momentum spectrum that is discretized in the simulation needs a finite set of basis states. The size of the momentum basis is defined in the parameter list. Further, the equation of motion in the momentum representation for the self-energy in second order approximation scales with $\mathcal{O}(N_b^3 N_t^1)$. This means the computation time scales linear with the number of time steps, but cubic with the number of momentum states. It should be noted that the larger the basis dimension is the more it converges to the true continuous spectrum. An adequate basis size needs to be found, so that the computation effort is still reasonable without giving up relevant precision. A simple method to investigate if the system converges is to let the same calculation run, with different basis sizes. The next step could be to look at the conserved quantities of each calculation and compare it. The conserved quantities are energy, particle number and particularly for translational invariant

systems, the momentum. If the conserving quantities do not change within the relevant precision, then the simulation converged. If the simulation does not converge, then this is an indication that the parameters are not chosen correctly, see figure 3.4. Additionally, one must decide which part of the momentum spectrum is relevant in the simulation and what part can be neglected, because of the computational limitation due to the finite basis size and the cubic basis scaling. That means, the part of the spectrum is chosen such that the particles do not propagate outside of the grid that is sampled. Also, the inverse screening length should not get smaller than the spacing between the sampled grid points, because that leads to more incorrect interaction effects, further, the energy does not converge the smaller the inverse screening length gets. The solution can be found when the basis size is increased or when GW self-energy is used, which has dynamical screening instead of the second Born approximation. If one makes the sampling grid wider, but does not adjust the basis dimension then the system is more vulnerable to numerical errors up to the point where it does not converge at all. It was observed that the error got too large so that the program crashed. That means caution is advised when parameters are chosen. Additionally, it was observed that when the thermodynamic beta is chosen too large then non-physical behaviors arise, like negative occupation numbers. It was observed that a larger basis, don't solve this problem. Since the equations scales cubic with the basis size, it is possible that the basis number was not increased sufficiently, to understand the difference.
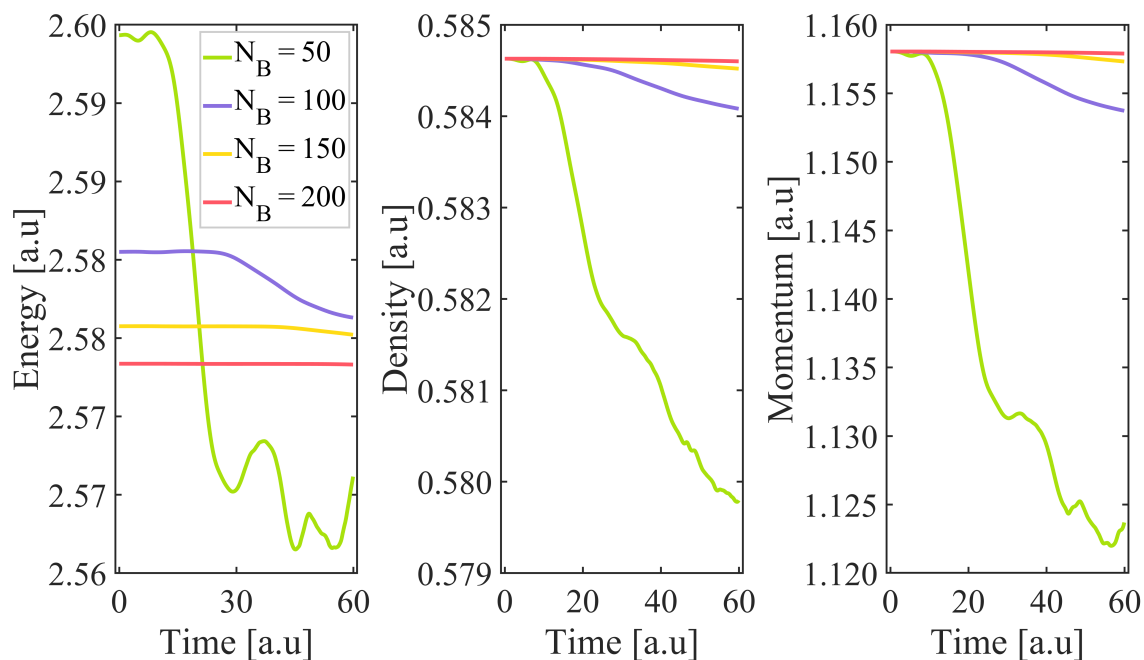

Figure 3.4: Convergence test for different Basis sizes N_B. For an ion bulk – ion beam configuration, see the blue curve of figure 4.3. On the left the energy, on the middle the density and on the right the momentum.

To verify some aspects of the convergence section, some conserved quantities are investigated for different basis sizes, see figure 3.4. It can be observed the conserved quantities converge, with increasing basis size. In comparison the red curve is constant over time for all figures. The yellow curve deviates, in the middle and right figure for large times. Whereas, in the left figure an energy offset is visible and the energy is also not constant for larger times. The same trend can be observed for the violet curve, the curve is just constant for the half period of time, and the energy offset in relation to the red curve is even larger. The green curve is not constant for any figure. Further, the energy is more sensitive to convergence, in contrast to density and momentum. That means, while in the middle and right figure all curves are on top of each other within the relevant precision, even though for a limited time span. The curves in the left figure have strongly visible offsets.

4 Results

At first, the aim of this thesis was the investigation of stopping power, in which a particle beam collides with an interacting system consisting of two different particle species, and then studying the energy loss of the beam. Unfortunately, the first calculations showed hardly any thermalization between the electrons of the beam and the electrons of the bulk, see figure 4.1. The green peak of the beam stays symmetric with time, no influence of the bulk can be observed. The red line of the beam, on the other hand, has an asymmetrical time evolution, the bulk seems to have an influence, scattering is observed. To explain the observed effects and in general the condition when the particles tend to collide became the primary objective of this thesis.
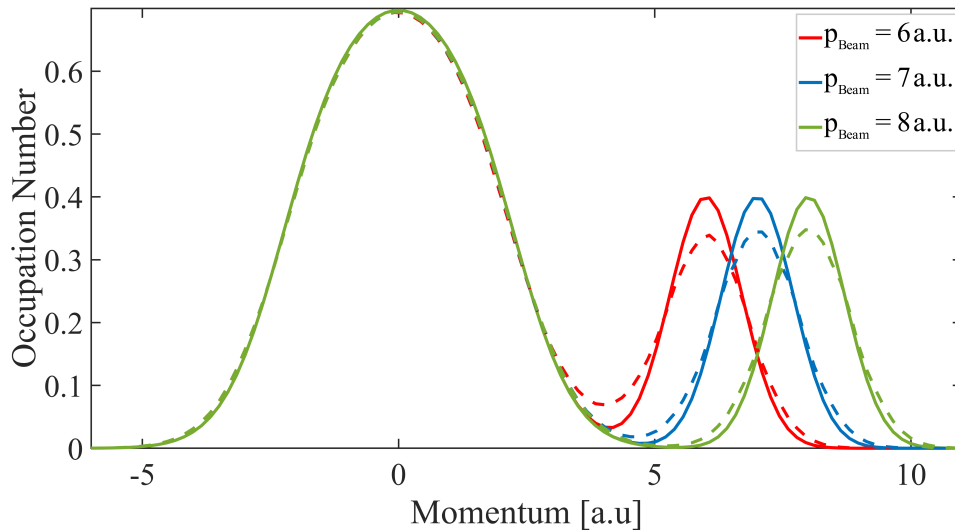
Figure 4.1: Momentum distribution of a one-dimensional one-component quantum wire. The three most right peaks are particle beams, interacting with the same color bulk of the system, the peak in the middle. The bulk and particle beam consist of electrons. The particle beam is set on different positions from the bulk. Solid line at initial time $t_i = 0$ a.u. and dashed line at final time $t_f = 60$ a.u.

4.1   Hypothesis

To study the dynamics of interacting multi-component system brought out of equilibrium through a particle beam, it is of the uttermost importance to know the condition in which collisions happen. The collision criterion will be derived in this section. We start with a hypothesis, followed by a proof in the form of a semi-analytical mathematical approach. Finally, the numerical results will be presented and discussed, to further support the hypothesis.

The hypothesis is the following:

"Particles with similar velocities are more likely to collide"

4.2   Derivation

To derive the collision criterion the GKBA for second Born self-energy is used.

We start with the equation of 1pNEGF, then the collision term take the following form

$$i\hbar\frac{d}{dt}G_\alpha^{<,\lambda}(\mathbf{k}_1,t) = [I + I^\dagger]_\alpha^\lambda(\mathbf{k}_1,t) =: \mathcal{I}_\alpha^\lambda(\mathbf{k}_1,t) \tag{4.1}$$

$$= 2\mathfrak{Re}\left\{I_\alpha^\lambda(\mathbf{k}_1,t)\right\} \tag{4.2}$$

$$= 2\mathfrak{Re}\left\{\int_{t_0}^t d\bar{t}\left[\Sigma^>(\mathbf{k}_1,t,\bar{t})G_\alpha^{<,\lambda}(\mathbf{k}_1,\bar{t},t) - \Sigma^<(\mathbf{k}_1,t,\bar{t})G_\alpha^{>,\lambda}(\mathbf{k}_1,\bar{t},t)\right]\right\}, \tag{4.3}$$

Then, equation (4.3) is evaluated for the case of fermionic species

$$\mathcal{I}_\alpha^\lambda(\mathbf{k}_1,t) = -2(i\hbar)^2\mathfrak{Re}\Bigg\{\int_{t_0}^t d\bar{t}\sum_{\substack{\beta\\\mu}}\int\frac{d\mathbf{k}_2}{(2\pi)^n}\int\frac{d\mathbf{q}}{(2\pi)^n}v^{\lambda\mu}(\mathbf{q},t)\Big(v^{\lambda\mu}(\mathbf{q},t') - v^{\lambda\lambda}(\mathbf{k}_1-\mathbf{q}-\mathbf{k}_2,t')\delta_{\alpha,\beta}\delta_{\lambda,\mu}\Big)$$

$$\times\Big(G_\alpha^{>,\lambda}(\mathbf{k}_1-\mathbf{q},t,\bar{t})G_\beta^{>,\mu}(\mathbf{k}_2+\mathbf{q},t,\bar{t})G_\beta^{<,\mu}(\mathbf{k}_2,\bar{t},t)G_\alpha^{<,\lambda}(\mathbf{k}_1,\bar{t},t) - (>\leftrightarrow<)\Big)\Bigg\}, \tag{4.4}$$

where the SOA self-energy was plugged in

$$\Sigma^{\gtrless}(\mathbf{k}_1,t,t') = \pm(i\hbar)^2\sum_{\substack{\beta\\\mu}}\int\frac{d\mathbf{k}_2}{(2\pi)^n}\int\frac{d\mathbf{q}}{(2\pi)^n}v^{\lambda\mu}(\mathbf{q},t)$$

$$\times\Big(v^{\lambda\mu}(\mathbf{q},t')\pm v^{\lambda\lambda}(\mathbf{k}_1-\mathbf{q}-\mathbf{k}_2,t')\delta_{\alpha,\beta}\delta_{\lambda,\mu}\Big) \tag{4.5}$$

$$\times G_\alpha^{\gtrless,\lambda}(\mathbf{k}_1-\mathbf{q},t,t')G_\beta^{\gtrless,\mu}(\mathbf{k}_2+\mathbf{q},t,t')G_\beta^{\lessgtr,\mu}(\mathbf{k}_2,t',t).$$

Then we reconstruct the off-diagonal 1pNEGF from diagonal ones with Hartree-Fock propagators.
The following expression will be obtained.

$$
\begin{aligned}
\mathcal{I}_\alpha^\lambda(\mathbf{k}_1, t) = &- 2(i\hbar)^2 \mathfrak{Re}\Bigg\{ \int_{t_0}^t d\bar{t} \sum_{\substack{\beta \\ \mu}} \int \frac{d\mathbf{k}_2}{(2\pi)^n} \int \frac{d\mathbf{q}}{(2\pi)^n} v^{\lambda\mu}(\mathbf{q}, t)\Big(v^{\lambda\mu}(\mathbf{q}, t') - v^{\lambda\lambda}(\mathbf{k}_1 - \mathbf{q} - \mathbf{k}_2, t')\delta_{\alpha,\beta}\delta_{\lambda,\mu}\Big) \\
&\times \Big(G_\alpha^{>,\lambda}(\mathbf{k}_1 - \mathbf{q}, \bar{t}, \bar{t})G_\beta^{>,\mu}(\mathbf{k}_2 + \mathbf{q}, \bar{t}, \bar{t})G_\beta^{<,\mu}(\mathbf{k}_2, \bar{t}, \bar{t})G_\alpha^{<,\lambda}(\mathbf{k}_1, \bar{t}, \bar{t}) - (> \leftrightarrow <)\Big) \\
&\times \exp\Big(-\int_{\bar{t}}^t d\tilde{t}\, \omega^{\mathrm{HF}}(\tilde{t})\Big)\Bigg\}
\end{aligned}
$$
(4.6)

$$
\begin{aligned}
= &-2(i\hbar)^2 \int_{t_0}^t d\bar{t} \sum_{\substack{\beta \\ \mu}} \int \frac{d\mathbf{k}_2}{(2\pi)^n} \int \frac{d\mathbf{q}}{(2\pi)^n} v^{\lambda\mu}(\mathbf{q}, t)\Big(v^{\lambda\mu}(\mathbf{q}, t') - v^{\lambda\lambda}(\mathbf{k}_1 - \mathbf{q} - \mathbf{k}_2, t')\delta_{\alpha,\beta}\delta_{\lambda,\mu}\Big) \\
&\times \Big(G_\alpha^{>,\lambda}(\mathbf{k}_1 - \mathbf{q}, \bar{t}, \bar{t})G_\beta^{>,\mu}(\mathbf{k}_2 + \mathbf{q}, \bar{t}, \bar{t})G_\beta^{<,\mu}(\mathbf{k}_2, \bar{t}, \bar{t})G_\alpha^{<,\lambda}(\mathbf{k}_1, \bar{t}, \bar{t}) - (> \leftrightarrow <)\Big) \\
&\times \cos\Big(-\int_{\bar{t}}^t d\tilde{t}\, \omega^{\mathrm{HF}}(\tilde{t})\Big)
\end{aligned}
$$
(4.7)

and $\hbar\omega^{\mathrm{HF}}(t) = h_\alpha^{\mathrm{HF},\lambda}(\mathbf{k}_1 - \mathbf{q})(t) + h_\beta^{\mathrm{HF},\mu}(\mathbf{k}_2 + \mathbf{q})(t) - h_\beta^{\mathrm{HF},\mu}(\mathbf{k}_2)(t) - h_\alpha^{HF,\lambda}(\mathbf{k}_1)(t)$.
From equation (4.6) to (4.7) the real part of the exponential is evaluated. Further, the two
times quantities are reconstructed with equation 2.34 and 2.35. In the following, to simplify
the collision term of the non-Markovian quantum Landau equation some assumptions need
to be made [4].
For short time scales the Fock energy is time-independent, which follows from the assumption
that the 1pNEGF is nearly constant. Thus, the time integral as the argument of cosine can
be evaluated

$$
\begin{aligned}
\mathcal{I}_\alpha^\lambda(\mathbf{k}_1, t) = &2\hbar^2 \int_{t_0}^t d\bar{t} \sum_{\substack{\beta \\ \mu}} \int \frac{d\mathbf{k}_2}{(2\pi)^n} \int \frac{d\mathbf{q}}{(2\pi)^n} v^{\lambda\mu}(\mathbf{q}, t)\Big(v^{\lambda\mu}(\mathbf{q}, \bar{t}) - v^{\lambda\lambda}(\mathbf{k}_1 - \mathbf{q} - \mathbf{k}_2, \bar{t})\delta_{\alpha,\beta}\delta_{\lambda,\mu}\Big) \\
&\times \Big(G_\alpha^{>,\lambda}(\mathbf{k}_1 - \mathbf{q}, \bar{t})G_\beta^{>,\mu}(\mathbf{k}_2 + \mathbf{q}, \bar{t})G_\beta^{<,\mu}(\mathbf{k}_2, \bar{t})G_\alpha^{<,\lambda}(\mathbf{k}_1, \bar{t}) - (> \leftrightarrow <)\Big) \\
&\times \cos\Big(-\omega^{\mathrm{HF}}(t - \bar{t})\Big).
\end{aligned}
$$
(4.8)

If the correlation Green's function relaxes much faster than the 1pNEGF, $\tau_{corr} \ll t_{relax}$ then
taking the Markov limit[4] is justified. Thus, during the time evolution of the correlation
Green's function, the 1pNEGF can be assumed time independent.

Further, the interaction matrix element is time-independent in this case, thus the time integral can be evaluated.

$$\int_{t_0-t}^{0} d\tau \, \cos\left(\omega^{HF}\tau\right) = \frac{\sin\left(\omega^{HF}(t-t_0)\right)}{\omega^{HF}}, \tag{4.9}$$

with $\tau = \bar{t} - t$.

Further, since $t - t_0 \gg \tau_{corr}$, one can take the limit $t_0 \to -\infty$

$$\lim_{t_0 \to -\infty} \frac{\sin\left(\omega^{HF}(t-t_0)\right)}{\omega^{HF}} = \pi\delta(\omega^{HF}), \tag{4.10}$$

where the property of the sinc function in relation to the Dirac delta function was exploited. Thus, the time-local quantum Landau integral is

$$\begin{aligned}
\mathcal{I}_\alpha^\lambda(\mathbf{k}_1,t) =& 2\hbar^2 \sum_{\substack{\beta \\ \mu}} \int \frac{d\mathbf{k}_2}{(2\pi)^n} \int \frac{d\mathbf{q}}{(2\pi)^n} v^{\lambda\mu}(\mathbf{q})\left(v^{\lambda\mu}(\mathbf{q}) - v^{\lambda\lambda}(\mathbf{k}_1 - \mathbf{q} - \mathbf{k}_2)\delta_{\alpha,\beta}\delta_{\lambda,\mu}\right) \\
&\times \left(G_\alpha^{>,\lambda}(\mathbf{k}_1 - \mathbf{q},t)G_\beta^{>,\mu}(\mathbf{k}_2 + \mathbf{q},t)G_\beta^{<,\mu}(\mathbf{k}_2,t)G_\alpha^{<,\lambda}(\mathbf{k}_1,t) - (> \leftrightarrow <)\right)\pi\delta\left(\omega^{HF}\right).
\end{aligned} \tag{4.11}$$

The change of rate of the 1pNEGF is a measure for dynamical behavior and scales, with the scattering probability, which is among other things, dependent on the argument of the delta function. Thus, the condition for which the delta function is $\neq 0$ must be looked into. The G1–G2 equation could have been used as well, to investigate the collision properties, but to evaluate the expression in a given approximation one has to deal with two equations of motions simultaneously. Analyzing just the EOM of correlation function is also possible but the interpretation of the solution is less obvious.

The general condition for $\omega^{HF} \to 0$ can be investigated with a Taylor series and expanded in powers of transfer momentum

$$\frac{\partial h_\beta^{\mathrm{HF},\mu}(\mathbf{k}_2)}{\partial \mathbf{p}_2} = \frac{\partial h_\alpha^{\mathrm{HF},\lambda}(\mathbf{k}_1)}{\partial \mathbf{p}_1}, \tag{4.12}$$

which expresses that the slope of the Hartree-Fock energies of the colliding particles need to compensate. When the kinetic energy dominates the dynamic of the system, which means $h_\alpha^{\mathrm{kin},\lambda}(\mathbf{k}_1) \gg h_\alpha^{\mathrm{Fock},\lambda}(\mathbf{k}_1)$ then $\omega^{\mathrm{HF}} \to 0$ with $h^{\mathrm{Fock}} \to 0$ yields

$$\hbar\omega^{\mathrm{HF}} \approx \mathbf{q}\left(\frac{\hbar^2\mathbf{k}_2}{m_\mu} - \frac{\hbar^2\mathbf{k}_1}{m_\lambda}\right) = \mathbf{p}_q\left(\frac{\mathbf{p}_2}{m_\mu} - \frac{\mathbf{p}_1}{m_\lambda}\right) \equiv \mathbf{p}_q(\mathbf{v}_2^\mu - \mathbf{v}_1^\lambda) =: \hbar\omega_{\Delta\mathbf{v}}^{\mathrm{kin}}, \tag{4.13}$$

with $\mathbf{p}_q = \hbar\mathbf{q}$, $\mathbf{p}_n = \hbar\mathbf{k}_n$ in which $n = 1, 2$ and all non-linear contributions were neglected. This implies the condition that particles, with the same velocity contribute to the dynamic of the system, when $\mathbf{v}_2^\mu = \mathbf{v}_1^\lambda$, then $\omega_{\Delta\mathbf{v}}^{\text{kin}} \to 0$ for $\mathbf{q} \to 0$. However, the derivation is formulated for the general case of three-dimensional space, nonetheless it is also valid for the two and one-dimensional space, but the conclusion is different concerning the collision criterion. In three- and two-dimensions the dot product of the transfer momentum $\mathbf{p}_q$, with the velocity difference plays a crucial role. A direction, in which the vectors are orthogonal to each other, always exists, which results in $\omega_{\Delta\mathbf{v}}^{\text{kin}} \to 0$ without $\mathbf{v}_2^\mu - \mathbf{v}_1^\lambda \to 0$. Therefore, it is expected that in three- and two-dimensions the collision criterion is not important. In one dimension, on the other hand the transfer momentum always has the same direction as the velocity difference. Thus, scattering can only be observed, when $\mathbf{v}^\mu - \mathbf{v}_1^\lambda \to 0$. It was already recognized in the investigation of optically excited semiconductors, that velocity is an important quantity to understand dynamical properties [20]. In this way plasmon damping can be better understood. Furthermore, this result is also known from classical plasma physics. When the relative velocity of colliding particles goes to zero, then the particle have more time to influence each other via field interaction. At this point, it should be noted that other factors can also influence the dynamics. In two or three dimensions the particles have more possibilities to evade each other, while in one dimension only one degree of freedom exists. Additional, it could be that the system was initialized close to stationary states, this could also slow down dynamics. Additionally, the inverse screening length also affects dynamics, the smaller this quantity gets the more scattering can be observed. Nonetheless, the velocity criterion is essential in this setup, it has the most influence, to the dynamic of the particles.

For further statements, lightweight particles are assumed, thus the Fock energy does not contribute to dynamics in comparison with the dominating kinetic energy. It is also assumed that particles in the bulk have a smaller momentum as particles in the beam. Because the velocity difference is a criterion, one needs to make a transition from momentum to velocity with $\mathbf{v} = \frac{\mathbf{p}}{m_\lambda}$. With this, the axis scales differently, for each different particle mass, which means the momentum distribution compresses with increasing mass. Thereby, colliding particles are closer to each other in velocity space, which means the relative speed of the colliding particles is small. Based on $\omega_{\Delta\mathbf{v}}^{\text{kin}} \to 0$ qualitative statements can be made.

- It is expected that for electron bulk electron beam interaction, the behavior will be comparative static, which is observed in figure 4.1.

- For ion bulk and ion beam interaction with increasing mass leads to a more dynamical behavior, because the bulk and beam is compressed.

- In case of ion bulk and electron beam there would not be any collisions, because just the ion bulk re-scales.

- For electron bulk and ion beam, some collisions will be observed between bulk and beam, again because the ion distribution re-scales.

4.3   Numerical Results

In this part of the thesis the collision criterion will be verified with numerical insight. Since the occupation number is an important quantity given by the solution of the G1–G2 scheme, it is reasonable to investigate it. Different bulk and beam configurations will be presented and their collision behavior will be discussed.

4.3.1   Electron Bulk – Electron Beam

We start with a series of one-component simulation, in figure 4.1, the momentum distribution of electrons is pictured for different beam peak positions. The solid same colored lines are at initial times $t_\mathrm{i} = 0$ a.u. and the dashed same color lines are at the final time $t_\mathrm{f} = 60$ a.u. of the simulation. Further, the radius of the wire is $r = 1$ a.u., the density is $n = \frac{1}{2}$ a.u. and the inverse temperature is $\beta_\mathrm{electron} = \frac{1}{2}$ a.u. We are particularly interested in the region between bulk- and beam peaks, because eventually in that interval collisions are most likely to be expected. It can be observed that the bulk for different line colors stays static in this setup, when one compares the initial and final time. The beam changes peak height with time. The particles in that region do not propagate significantly outside their respective original peak position, but the probability increases slightly for example between bulk and the beams. That means in that momentum interval, the particles collide. Further, beams that are closer to the bulk collide more with each other in contrast to the beam that is further away, but overall there is not much change. The particles of the bulk and the beam do not scatter a lot.

The explanation can be found in section 4.2. The momentum is proportional to the velocity of the particles, that means that not much dynamics are seen in the figure, because most particles collides with the immediate surroundings in velocity space. The bulk collide with particles in the bulk and the same happens for the particles in the beam, they collide with the particles in the beam. Except when the beam is close enough to the bulk, then the transfer momentum is small and the velocity difference between bulk and beam goes to zero and interaction happens, demonstrated with the increase in occupation number in that region.
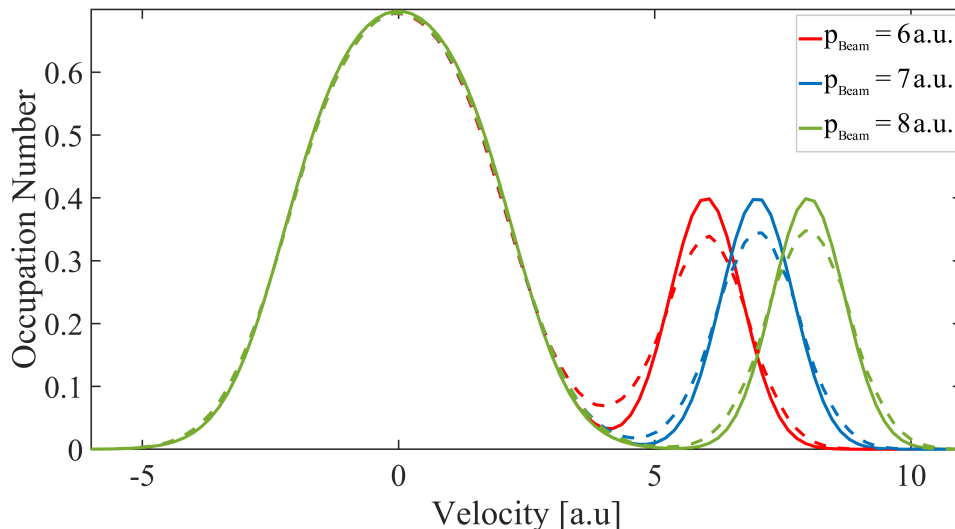
Figure 4.2: Velocity distribution of a one-dimensional one-component quantum wire. The three most right peaks are particle beams, interacting with the same color bulk of the system, the peak in the middle. The bulk and particle beam consist of electrons. The particle beam is set on different positions from the bulk. Solid line at initial time $t_i = 0$ a.u. and dashed line at final time $t_f = 60$ a.u.

4.3.2   Ion Bulk − Ion Beam

The second series of one-component calculations, figure 4.3, the momentum distribution for ions of arbitrary mass is pictured for the same beam peak position. The same time span as before is investigated. Further, the particles are initialized with the same wire radius and density as before. The ions possess an inverse temperature of $\beta_{\text{ion}} = 1$ a.u.. It can be seen that the bulk for different solid line color changes the form with increasing mass due to the decreasing dispersion that influences the Fermi Hartree-Fock initialization. The same trend can be seen for the particle beam. The beam height changes and the distribution spreads more the heavier the particle species is. For the red line, it behaves like in figure 4.1, it stays static. The blue line on the other hand decreases with time for the bulk and beam. Thus, the occupation number propagates outside of their initial peak position, especially to the valley between bulk and beam and populates other momentum states.

The green line follows the trend of the blue distribution, but decreases further in height in time and spreads further, as far as at final time there is no second local maximum. So the particles in the green line distribution scatter the most and the particles in the red line distribution scatter the least.
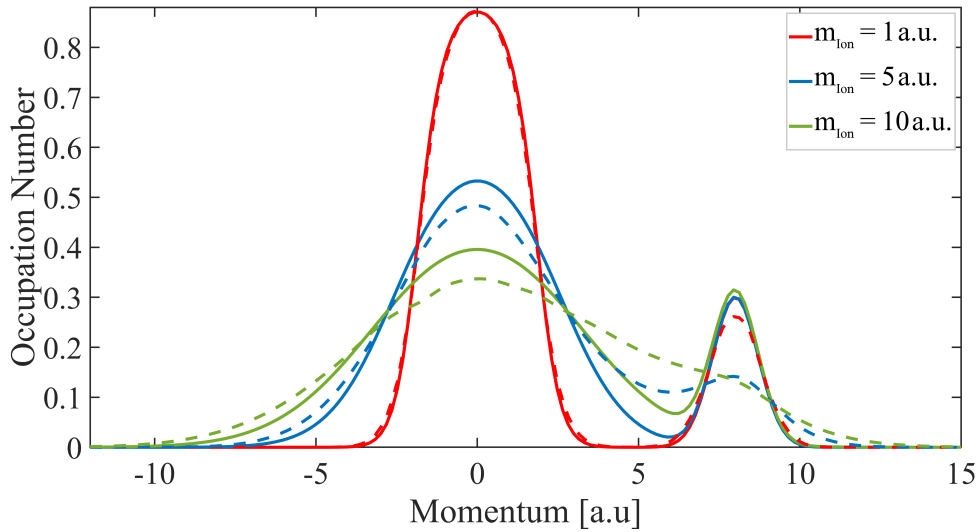
Figure 4.3: Momentum distribution of a one-dimensional one-component quantum wire. The peak on the right is the particle beam, interacting with the same color bulk of the system, the peak in the middle. The bulk and particle beam consist of ions. The particle beam is set on one fixed position and the mass is varied to study the strength of the dynamics. Solid line at initial time $t_i = 0$ a.u. and dashed line at final time $t_f = 60$ a.u.

The previous explanation holds. The occupation number compresses proportional to the mass of the particle type, see figure 4.4. Therefore, the green line the bulk interaction range is wider than the other lines, because in the transition from momentum to velocity the bulk beam occupation number is closer to each other in velocity space. That means for particles with a mass of 10 a.u. the occupation numbers are 10 times closer to each other in velocity space in comparison to momentum space. If we observe the transition from momentum to velocity for the red line, the bulk still seems far away from the beam in velocity space.
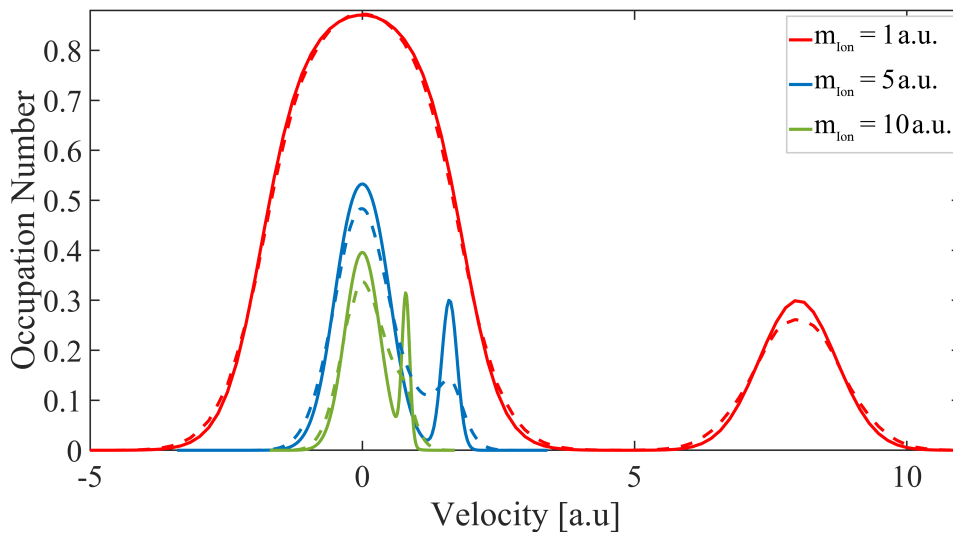

Figure 4.4: Same as 4.3, just against velocity instead of momentum.

4.3.3   Electron Bulk – Ion Beam

The third series of calculations will be a two-component case, see figure 4.5. The momentum distribution consisting of an electron bulk and ion beam for fixed beam position but with varied ion mass. The same time span as before is investigated. The wire radius and density stays the same as before. The inverse temperature of the particles are as follows $\beta_{\text{electron}} = \frac{1}{2}$ a.u. and $\beta_{\text{ion}} = 1$ a.u.. The occupation number of the beam spreads more around the peak, the higher the mass of the particle is, like in figure 4.3. Further, the electron bulk scattering with the ion beam increases, with larger ion mass. The red line behaves similarly to figure 4.1, it stays static, the same trend is seen in the red lined beam. The blue line electron bulk shows some disturbance. The occupation number warps to the right in the direction of the ion beam. The ion beam spreads to the outside with tendency in direction to the electron bulk, like in figure 4.1. The occupation number of the same color bulk and beam cross, because they can populate the same momentum and spin quantum states. The green line follows the trend of the blue distribution, again with tendency to the ion beam. The ion beam behaves in a similar manner as the blue beam curve with a tendency to the left in the direction of the electron bulk. The same argument for Pauli blocking holds.
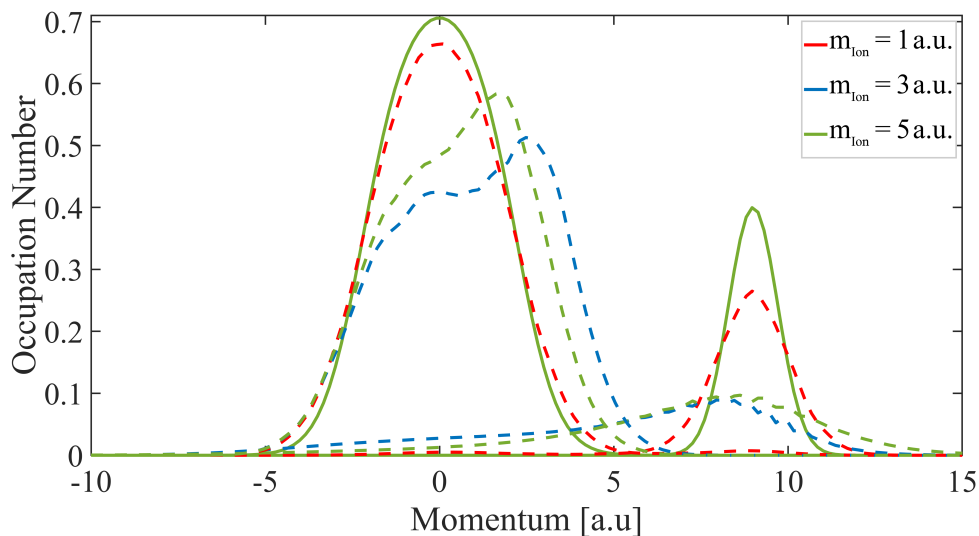

Figure 4.5: Momentum distribution of a one-dimensional two-component quantum wire. The peak on the right is the particle beam, interacting with the same color bulk of the system, the peak in the middle. The bulk consists of electrons and particle beam consists of ions. The particle beam is set on one fixed position and the mass is varied to study the strength of the dynamics. Solid line at initial time $t_{\text{i}} = 0$ a.u. and dashed line at final time $t_{\text{f}} = 60$ a.u.

The velocity is proportional to the momentum and inverse proportional to the mass of the particle, $\mathbf{v} = \frac{\mathbf{p}}{m_\lambda}$. As before the compression is proportional to the mass of the particles, see figure 4.6. Therefore the red curve behaves similar to the electron beam electron bulk

calculations. Whereas the blue and green curve of the beam are close to the electron bulk in velocity space. That explains the deformation of the electron bulk to the right. In velocity space the shape of the bulk does not change. In contrast to the blue and green beam distribution in velocity space, the respective beams are exactly below the disturbance of the electron bulk, that means $\mathbf{v}^\mu - \mathbf{v}_1^\lambda \to 0$, thus collision can be observed.
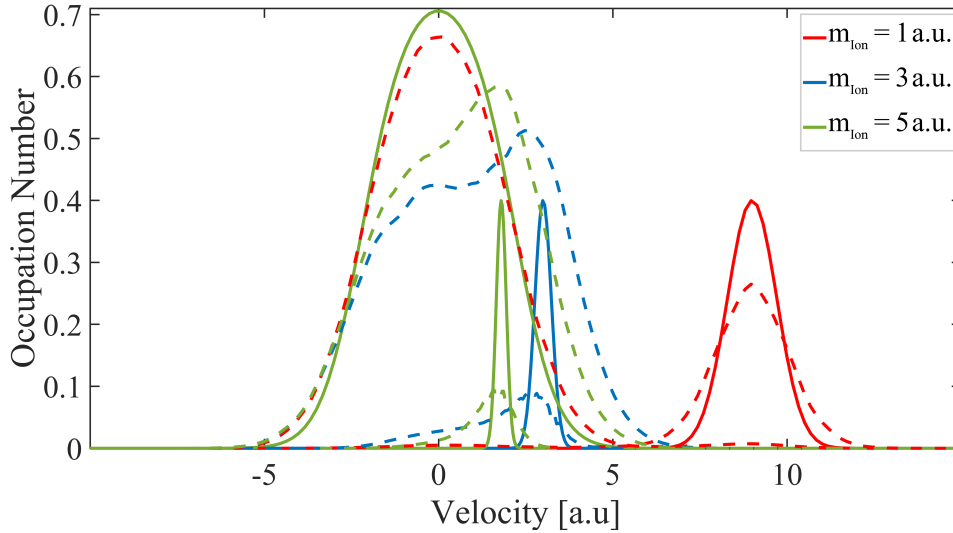

Figure 4.6: Same as 4.5, just against velocity instead of momentum.

4.3.4 Ion Bulk – Electron Beam

The fourth and last series of calculations will be examined. The two-components system consists of an ion bulk and electron beam, see figure 4.7 for fixed beam position but different particle bulk masses. The same time span, wire radius, density and inverse temperature as before is investigated. The beam and bulk relaxate slightly when one compares the solid lines with the dashed line. The particles of the bulk just scatter with other particles in the bulk and the beam just scatter with other particles in the beam. Overall no collision between bulk and beam can be observed.
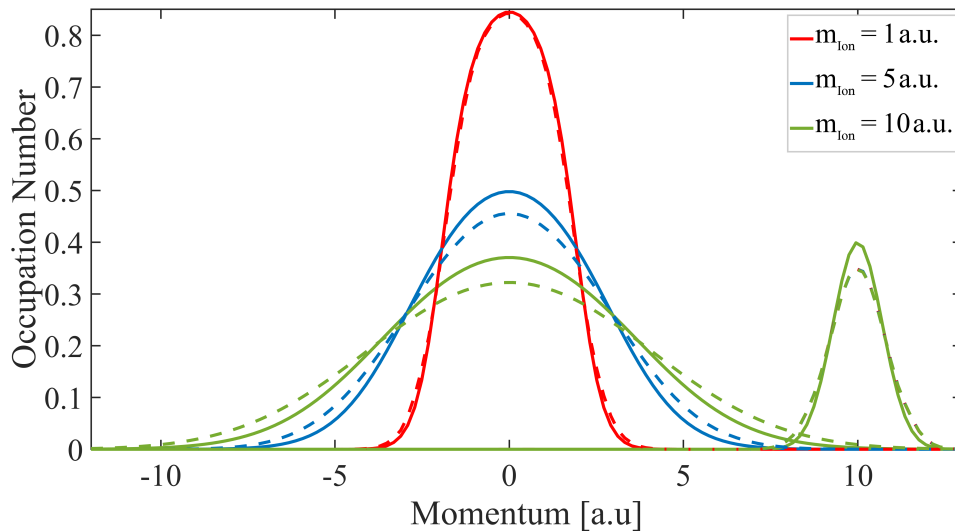
Figure 4.7: Momentum distribution of a one-dimensional two-component quantum wire. The peak on the right is the particle beam, interacting with the same color bulk of the system, the peak in the middle. The bulk consists of ions and particle beam consists of electrons. The particle beam is set on one fixed position. The mass of the bulk is varied to study the strength of the dynamic. Solid line at initial time $t_\mathrm{i} = 0$ a.u. and dashed line at final time $t_\mathrm{f} = 60$ a.u.

The reason for this behavior can be found again with the same argument as before see figure 4.8. The velocity difference does not approach zero between bulk and beam. In velocity space the red lined bulk is closest to the bulk, but the occupation number of the bulk and beam do not cross. With increasing mass the tendency for collisions to happen get worse because the blue and green bulk line is even further away in velocity space, from the electron beam this way the criterion for collisions is not fulfilled.
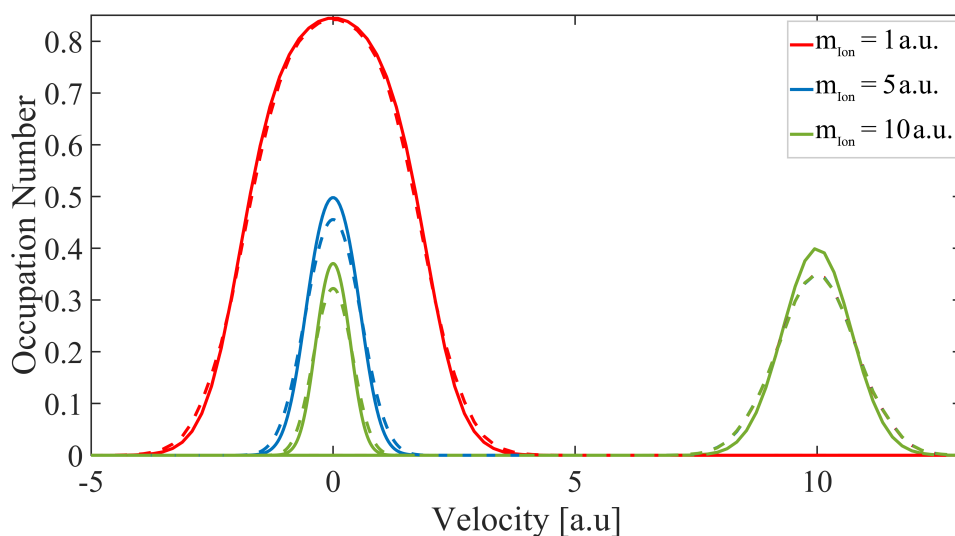

Figure 4.8: Same as 4.7, just against velocity instead of momentum.

5 Conclusion & Outlook

In this thesis the collision criterion for a one-dimensional two-component quantum plasma described with the kinetic equations of the G1–G2 scheme in second Born approximation was investigated. The simulation consisted of two bulks associated with two particle species and a particle beam. Different bulk beam plasma configurations were investigated and it could be shown that the behavior of the simulations is in agreement with the condition $\omega_{\Delta v}^{\text{kin}} \to 0$, which implies that the velocity difference plays a crucial role when it comes down to dynamical behavior. Further, it could be shown that the G1–G2 scheme works well enough for a continuous basis set in one dimension.

Outlook

The next step could be to test higher order self-energies and investigate if the condition $\omega_{\Delta v}^{\text{kin}} \to 0$ breaks, the reason behind the possibility lies in the different mathematical structure of the different self-energies. Further, because of the multi-component structure of the equations, the modification to a multi-band system is a small step. One needs to replace the diagonal species indices with non-diagonal band indices. The transition to two-dimensions or even three dimensions could be more reasonable, because in one-dimension the practical use is more limited. Then more realistic stopping simulations can be made, such as investigations of α-particles at low projectile velocities near the Bragg peak, to better understand inertial confinement fusion and the energy transfer of the ions to the hydrogen pellet. Returning to the one-dimensional system in this thesis: Because the condition for which particles collide is better understood, the original reason of this thesis, stopping power calculations, can also be investigated. In fact, following the investigation in this thesis, first stopping power calculations were analyzed [21].

Bibliography

[1] Niclas Schlünzen, Jan-Philip Joost, and Michael Bonitz. "Achieving the Scaling Limit for Nonequilibrium Green Functions Simulations". In: *Physical review letters 124, 076601* (2020).

[2] Jan-Philip Joost, Niclas Schlünzen, and Michael Bonitz. "The G1–G2 Scheme: Dramatic Acceleration of Nonequilibrium Green Functions Simulations Within the Hartree-Fock-GKBA". In: *Phys. Rev. B 101, 245101* (2020).

[3] Michael Bonitz, Norman Horing, and Patrick Ludwig. *Introduction to Complex Plasmas (Springer Series on Atomic, Optical, and Plasma Physics, 59, Band 59).* Springer, 2010.

[4] Michael Bonitz. *Quantum Kinetic Theory.* Springer, 2016.

[5] Karsten Balzer, Maximilian Rodriguez Rasmussen, Niclas Schlünzen, Jan-Philip Joost, and Michael Bonitz. "Doublon formation by ions impacting a strongly correlated finite lattice system". In: *Phys. Rev. Lett. 121, 267602* (2018).

[6] Lotte Borkowski, Niclas Schlünzen, Jan-Philip Joost, Franziska Reiser, and Michael Bonitz. "Doublon production in correlated materials by multiple ion impacts". In: *arXiv:2110.06644v1 [cond-mat]* (2021).

[7] Michael Bonitz, Dietrich Kremp, S. Kosse, D.C Scott, and Wolf Dietrich Kraeft. *Influence of many-particle effects on stopping power.* World Scientific, 1996.

[8] Zhandos Moldabekov, Tobias Dornheim, Michael Bonitz, and Tlekkabul Ramazanov. "Ion energy-loss characteristics and friction in a free-electron gas at warm dense matter and nonideal dense plasma conditions". In: *Phys. Rev. E 101, 053203* (2020).

[9] Erwin Schrödinger. "Quantisierung als Eigenwertproblem (Erste Mitteilung)". In: *Annalen der Physik, (4), 79, 361-376* (1926).

[10] Paul Adrien Maurice Dirac. *The Principles of Quantum Mechanics.* Oxford University Press, U.S.A., 1988.

[11] Leo Philip Kadanoff and Gordon Alan Baym. *Quantum Statistical Mechanics.* Westview Press, 1962.

[12]   Leonid Veniaminovich Keldysh. "Diagram technique for nonequilibrium processes". In: *Sov. Phys. JETP, 20:1018* (1965).

[13]   Freya Schüler. *Image reconstruction with Photoshop.* 2021.

[14]   Karsten Balzer and Michael Bonitz. *Nonequilibrium Green's Functions Approach to Inhomogeneous Systems.* Springer, 2012.

[15]   Paul Cecil Martin and Julian Seymour Schwinger. "Theory of Many-Particle Systems I". In: *Phys. Rev. 115, 1342* (1959).

[16]   Gianluca Stefanucci and Robert van Leeuwen. *Nonequilibrium Many-Body Theory of Quantum Systems: A Modern Introduction.* Cambridge University Press, 2013.

[17]   Pavel Lipavský, Václav Špička, and Bedřich Velický. "Generalized Kadanoff-Baym ansatz for deriving quantum transport equations". In: *Phys. Rev. B 34, 6933* (1986).

[18]   Jun John Sakurai. *Modern Quantum Mechanics.* Cambridge University Press, 2020.

[19]   Gabriele Giuliani and Giovanni Vignale. *Quantum Theory of the Electron Liquid.* Cambridge University Press, 2005.

[20]   M. Bonitz, J. F. Lampin, F. X. Camescasse, and A. Alexandrou. "Nonequilibrium plasmons in optically excited semiconductors". In: *Phys. Rev. B 62, 15724* (2000).

[21]   Christopher Makait, Francisco Borges Fajardo, Niclas Schlünzen, Jan-Philip Joost, and Michael Bonitz. "Time-resolved stopping power in dense quantum plasmas: a Green's Functions approach". In: *Physics of Nonideal Plasmas 17 (PNP17), Poster Session Thursday* (2021).

Danksagung

Abschließend spreche ich meinen Dank, den Menschen aus, die diese Arbeit möglich gemacht haben.

Zuallererst Prof. Dr. Michael Bonitz, welcher mir die Möglichkeit gab mich weiterzuentwickeln und mir durch Seine Unterstützung Sicherheit und Motivation zuteilwerden ließ.

Ebenfalls möchte ich Christopher Makait, für die anregenden Gespräche und die gute Betreuung, danken. Er hatte immer ein offenes Ohr für mich, dies weiß ich sehr zu schätzen.

Eigenständigkeitserklärung

Hiermit erkläre ich, dass ich die vorliegende Arbeit selbständig und ohne fremde Hilfe angefertigt und keine anderen als die angegebenen Quellen und Hilfsmittel verwendet habe.

Weiterhin versichere ich, dass diese Arbeit noch nicht als Abschlussarbeit an anderer Stelle vorgelegen hat.

_____

Datum, Unterschrift